# Artificial Diagenesis of Carbonates: Temperature-Dependent Inorganic and Organic Modifications in Reservoir Mimetic Fluids

**Ashit Rao, Saravana Kumar, Carla Annink,** and **Duy Le-Anh,** Physics of Complex Fluids Group and MESA+ Institute, University of Twente; **Subhash C. Ayirala** and **Mohammed B. Alotaibi,** The Exploration and Petroleum Engineering Center—Advanced Research Center (EXPEC ARC), Saudi Aramco; **Igor Siretanu** and **Michel H. G. Duits,** Physics of Complex Fluids Group and MESA+ Institute, University of Twente; **Ali A. Yousef,** The Exploration and Petroleum Engineering Center—Advanced Research Center (EXPEC ARC), Saudi Aramco; and **Frieder Mugele,** Physics of Complex Fluids Group and MESA+ Institute, University of Twente

## Summary

Within reservoirs, spatial variations related to mineralogy and fluid chemistry determine the success of improved oil recovery (IOR) technologies. However, the composition and structure of mineral-adsorbent/fluid interfaces, which fundamentally determine the wettability of reservoir rocks and crude oil (CRO) displacement, are unclear. Replicating the diagenetic alterations of carbonates, this study addresses the temperature dependence of the inorganic and organic modifications of calcite by reservoir pertinent fluids as well as its consequences on mineral wettability and reactivity.

We apply a suite of characterization methods, namely confocal Raman, scanning electron, and atomic force microscopy (AFM) as well as infrared spectroscopy, to investigate the modifications of carbonates on aging in formation water (FW), CRO-equilibrated FW, and FW-equilibrated CRO. The microscopic modifications of carbonates show a strong dependence on the aging temperature and are varied, encompassing topographical alterations, substitution of lattice $Ca^{2+}$ ions by $Mg^{2+}$ ions and the deposition of particles enriched with polyaromatic hydrocarbons (PAHs) as organic adlayers. Aging in the FWs leads to substantial reconstruction of calcite surfaces, with the deposition of magnesium calcite layers at elevated temperatures. Subsequent aging in FW-equilibrated CRO produces an organic coating on the mineral surfaces, which is composed of PAH-enriched particles. Deposited most strongly at high temperature, these organic layers render contact angles more "oil-wet." In addition, these layers present a limited permeability for ionic species and substantially reduce the dissolution rates of calcite. The multilayer deposition of organic particles, which thus turns out as a key factor for wettability alteration, is attributed to the interconnected bulk and surface reactions for interfacially active constituents of CRO and the surface precipitation of organo-calcium complexes.

Results of this study are relevant to multiple aspects of reservoir development and maintenance, including laboratory scale wettability and coreflooding experiments, and in-silico modeling. The observed nano- and microscopic surface alterations of carbonates within reservoir mimetic environments improve our understanding of the physicochemical relations between mineralogy and fluid chemistry at the mineral-sorbent/fluid interfaces within reservoirs and thereby provide a starting point for the development of novel advanced IOR strategies.

## Introduction

Accounting for more than half of Earth's oil (Klemme and Ulmishek 1991), carbonate reservoirs represent an important energy resource. Yet oil production from such reservoirs remains a strong challenge and can rely on IOR technologies, such as low-salinity water, surfactant, and polymer flooding (Yousef et al. 2011; Shah 2012). An important parameter in the development of oil reservoirs is wettability, which in turn affects the flow behavior and displacement of fluids in porous rock media (Abdallah et al. 1986; Morrow 1990). Preferentially oil-wet rock formations result in high residual oil saturation. Yet, the fundamental microscopic aspects of reservoirs, which determine mineral wettability, remain unclear. It is essential to address this knowledge gap to improve our understanding of the complex dynamics of oil/brine/mineral systems and also to strategically develop and deploy novel IOR technologies.

Physicochemical properties of minerals represent an important link between the geology and engineering of reservoirs (Larter et al. 1997; Peters and Fowler 2002). Addressing the geological origins of initial oil-wet or mixed-wet states of reservoir formations, studies have shown that certain CRO components chemically or physically adsorb on carbonate surfaces (Frye and Thomas 1993; Piro et al. 1996; Yu and Buckley 1997; Alhammadi et al. 2017; Sørgård et al. 2017). Although it is widely accepted that the organic modifications of minerals determine wetting characteristics, different findings have been made on the chemical identity of adsorbing species as well as the composition and structure of resulting mineral-adsorbent/fluid interfaces. For instance, long-chain fatty acids, asphaltenes, resins, naphthenic acids, kerogens, and carbazoles have all been suggested as adsorbents on mineral surfaces (Frye and Thomas 1993; Piro et al. 1996; Subramanian et al. 2017; Al-Busaidi et al. 2019). Because of this array of proposed CRO-derived adsorbents, the microscopic mechanisms that govern initial wettability and IOR-induced alterations remain ambiguous. To address this uncertainty, it is necessary to characterize the interactions and interfaces in reservoir pertinent oil/brine/mineral systems, focusing on both composition and structure.

Synthetic replication of reservoir-relevant oil/brine/mineral systems can facilitate the understanding of the in-situ chemical and topographical properties of minerals (Chen et al. 2017; Rao et al. 2020). For this, certain key factors require attention, such as the equilibration



This paper (SPE 200331) was accepted for presentation at the SPE Improved Oil Recovery Conference, originally scheduled to be held in Tulsa, Oklahoma, USA, 18–22 April 2020, and revised for publication. Due to COVID-19, the physical event was postponed until 31 August–4 September and was changed to a virtual event. The official proceedings were published online 30 August 2020. Original manuscript received for review 30 March 2020. Revised manuscript received for review 16 July 2020. Paper peer approved 20 July 2020.

of CRO and reservoir brines at geological scales as well as the diagenetic alterations of minerals at elevated temperature and pressure. For instance, some water-soluble constituents of CRO can migrate to connate waters within reservoirs (Hutin et al. 2014; Eftekhardadkhah et al. 2016). This affects the composition of reservoir fluids and, in turn, possibly the organic and inorganic modifications of minerals as well. Within the pools of CRO and brines, the diagenesis of mineral phases influences the wettability, porosity, and permeability of reservoirs (Moore 1989; Moore and Wade 2013). Diagenetic processes also determine the contents of Mg-calcite and dolomite within formations, which significantly affect reservoir characteristics and performance (Schmoker et al. 1985; Sun 1995). Over geological time scales, these mineral/fluid reactions can yield (metastable) equilibrium conditions (Helgeson et al. 1993). Experimental simulations of diagenesis in the laboratory, creating the possibility of such processes to occur, can help address open questions about the nature of surface-active species and their relative organization at oil/brine/mineral interfaces (Larter et al. 1997; Buckley 2001; Chen et al. 2017; Joonaki et al. 2019).

Here, one aspect that is often underilluminated in laboratory studies is the lack of uniformity in real reservoirs. Geochemical appraisals of reservoirs often report significant spatial gradients of mineral and fluid compositions. Within the same field, depth-dependent variations in mineral compositions for limestone, dolomite, and anhydrite are reported (Cantrell et al. 2004; Hong et al. 2016). Compositional variations of fluids within a single oil pool in reservoirs have been reported and attributed to thermal gradients and gravity (Hirschberg 1988; Montel et al. 2003; England 2007). For instance, tar mats (asphaltene-rich zones of heavy oil) are sometimes found at the bottom of reservoirs and pose a challenge toward the development of oil reservoirs. At present, we lack the understanding of the formative processes leading to these compositional gradients, including the associated rates and magnitudes. Moreover, several experimental studies use pristine mineral surfaces at ambient temperature and pressure conditions, and thereby exclude key physicochemical aspects of reservoir environments. Coreflooding experiments routinely aim at mimicking reservoir conditions by exposing mineral surfaces to CRO and brines following well-defined aging protocols (Anderson 1986; Jadhunandan and Morrow 1995; Jackson et al. 2016). However, these aging protocols vary substantially between different laboratories, and their usefulness and reliability are generally only assessed by macroscopic tests. Their consequences for the microscopic structure and composition of the mineral surfaces are hardly ever characterized in detail, in sharp contrast to the fact that these microscopic properties are widely believed to control wettability (Chen et al. 2017; Rao et al. 2020). To achieve a consistent fundamental picture and also an understanding of waterflooding and more advanced IOR techniques in carbonate reservoirs, it is therefore essential to achieve a thorough microscopic picture of the processes controlling the properties of the oil/brine/mineral interfaces under realistic reservoir conditions.

In this study, we provide a first step toward this goal by characterizing the microscopic alterations of carbonate surfaces upon exposure to reservoir pertinent connate water and CRO at temperatures up to 95°C using a suite of techniques, namely optical microscopy, scanning electron microscopy (SEM), Fourier transform infrared spectroscopy (FTIR), confocal Raman microscopy, and AFM, complemented by macroscopic contact-angle goniometry. While each of these techniques has been applied before, the combination of the complementary results illustrates in a unique manner the subtle balance of competing processes that control the properties of the oil/brine/mineral interface and how dramatically this balance is altered at elevated temperature. Any microscopic understanding of IOR techniques should be based on the shifts of these delicate equilibria.

## Experimental Section

**Materials.** Rock specimen and batches of dead CRO were obtained from a carbonate reservoir. As summarized in Table S1 (referring to the supporting information provided with this paper), the characterization of CRO was performed by a certified laboratory of Saybolt Nederland BV, and the viscosity was measured with a Thermo Scientific Haake™ RheoStress™ 600 controlled-stress rheometer. Mineral samples used in laboratory experiments were freshly cleaved Iceland spar (Ward's Scientific, Henrietta, New York, USA) and calcite powders (Sigma-Aldrich, St. Louis, Missouri, USA). Artificial FW (or "unaged FW") was prepared by mixing reagent-grade chemicals (calcium chloride, magnesium chloride, magnesium sulfate, sodium chloride, and sodium bicarbonate) (Sigma-Aldrich) with deionized water (18.2 MΩ cm; Milli-Q®, Millipore Sigma, Burlington, Massachusetts, USA), to attain a defined composition **(Table 1).** The brine composition is based on the chemical analysis of field water samples from a carbonate reservoir (Yousef et al. 2011). At room temperature (RT), the mixture was stirred overnight and filtered through a polyethersulfone (or PES) filter membrane (0.45 μm).

| | | |
|---|---|---|
| $Na^+$ | Cations (ppm) | 59,491 |
| $Ca^{2+}$ | | 19,040 |
| $Mg^{2+}$ | | 2,439 |
| $SO_4^{2-}$ | Anions (ppm) | 350 |
| $Cl^-$ | | 132,060 |
| $HCO_3^-$ | | 354 |
| Total dissolved solids | (ppm) | 213,734 |
| Ionic strength | | 4.31 |
| pH | | 6.8 |

Table 1—Composition and geochemical analysis of artificial FW.

**FW/CRO Equilibration.** To mimic the equilibration of aqueous fluids and CRO at elevated temperatures within reservoirs, a previously described protocol was followed (Rao et al. 2020). In brief, equal parts of CRO and FW were equilibrated at 95°C for 48 hours. Prior to equilibration, Iceland spar crystals were added to the mixture for pH maintenance. To assist solute transfer between the fluids while avoiding emulsion formation, intermittent gentle shaking was applied in course of equilibration. After equilibration and cooling to RT, the brine (eqFW) and oil (eqCRO) phases were separated, stored in sealed glass bottles, and used within 2 weeks of preparation.

**Surface Modification of Calcite.** The surface modification of freshly cleaved Iceland spar crystals in the equilibrated fluids was performed in a sequential manner (Fig. S1). The crystals were initially aged in FW or eqFW for 16 hours and then in eqCRO for 7 days. The aging procedure was applied at either RT (approximately 21°C), 60°C, or 95°C. Preceding surface characterization, the FW- or eqFW-aged crystals were briefly rinsed with deionized water to avoid salt formation by evaporative processes. For eqCRO-aged crystals (initially treated with eqFW), the substrates were gently cleaned with a toluene stream, which assisted the removal of oil residues. The

aged calcite samples were dried overnight in a fume hood, stored in a nitrogen box at RT, and used within 4 weeks of preparation. Similar surface modification protocols were applied to calcite powders (Fig. S2).

**Molecular and Microscopic Characterizations.** Confocal Raman microscopy was performed using a WITec alpha300 R instrument equipped with a 532 nm excitation laser. A spectral resolution of approximately 2.3 $cm^{-1}$ was provided by a grating of 600 g/mm. A 50X objective (Zeiss EC Epiplan with numerical aperture $=0.75$) and a charge coupled device (CCD) camera ($1600 \times 200$ pixels, 16 μm pixel size; Andor Newton, Concord, Massachusetts, USA) were used. Baseline correction was performed by using the WITec ProjectFIVE software and then a principal component analysis (PCA)-guided denoising algorithm was applied (Fig. S3) (Nair et al. 2020). To generate Raman maps, the spectral regions of interest were integrated for each pixel: from 1076 to 1095 $cm^{-1}$ for Iceland spar calcite ($\nu_1$, in-plane bending), from 1084 to 1097 $cm^{-1}$ for calcite ($\nu_1$, in-plane bending) from reservoir rock specimens, and 1500 to 1650 $cm^{-1}$ for PAHs (G and D2 bands). Residuals obtained from baseline correction were used to localize fluorophores. SEM was performed with a Zeiss MERLIN HR-SEM instrument equipped with a module for energy-dispersive X-ray spectroscopy. AFM imaging via amplitude modulation was performed at a rate of 0.5 Hz with resolution of $512 \times 512$ in air using NSC36 probes (MikroMasch, Watsonville, California, USA) and a Bruker Dimension Icon instrument. 3D images of the fluorescence distributions were acquired by using a VisiTech Infinity3 confocal scanning laser microscope (CSLM) with a 488 nm excitation laser, 60× objective, and an ORCA Flash 2.8 camera at $2 \times 2$ binning (Hamamatsu Corp., Bridgewater, New Jersey, USA). Z stacks were obtained with step sizes of 1 μm, and maximum pixel intensity values for each Z-slice were used to generate intensity profiles as a function of depth.

For calcite powders, FTIR spectra were acquired with a Bruker alpha spectrometer operated in attenuated total reflection mode. The kinetics of calcite dissolution was assessed by monitoring the development of free $Ca^{2+}$ ions upon addition of mineral powders (50 mg) to deionized water (50 $cm^3$) maintained at a constant temperature (40°C). Evolution of the $Ca^{2+}$ ion concentration was monitored using a combination ion selective electrode (HI-4104) and a HI-931 potentiometric system (Hanna Instruments, Woonsocket, Rhode Island, USA). The Guggenheim approach was used to evaluate the rate constants for calcite dissolution (Niebergall and Sugita 1968).

**Contact-Angle Measurements.** Contact-angle goniometry was used to characterize the wettability of eqCRO-aged Iceland spar surfaces at RT. In ambient eqFW, contact angles of eqCRO droplets were estimated by using a Dataphysics OCA 20L instrument via the captive bubble method. A steel needle, used for automated dispensing of eqCRO, was immersed in eqFW in a glass cuvette (Hellma Analytics, Plainview, New York, USA). The calcite substrate was immersed in the ambient brine for 30 minutes, which provided for some equilibration. The experiment was initialized by dispensing a 5-μL drop of eqCRO on the substrate. After 30 minutes, the eqCRO droplet was infused at a rate of 0.015 μL/min to a final drop volume of 20 μL. During infusion, the angle between the mineral surface and the brine/eqCRO interface was monitored. The receding contact angle ($\theta^{rec}_{brine}$) was estimated. However, the advancing contact angles ($\theta^{adv}_{brine}$) could not be accurately estimated. Several droplet and substrate replicates, with approximately two to three droplets for each Iceland spar sample, were made to obtain representative $\theta^{rec}_{brine}$ values.

## Results and Discussion

**Inorganic and Organic Modifications of Reservoir Rocks.** Petrographic characteristics of reservoir rocks underlay the efficacy of IOR processes. One of the nondestructive methods applied for characterizing reservoir materials is Raman spectroscopy (Jehlička et al. 2003; Khatabi et al. 2018). For example, unique spectral features exhibited by different carbonaceous matter enable the structural characterization of rock-associated organic molecules (Jehlička et al. 2003). However, the acquisition of spatially resolved information from confocal Raman datasets is more demanding and requires effective signal processing. In particular, contributions from fluorescence emission and instrumental noise to the spectral data require attention. As shown in Fig. S3, the fluorescence background is a distinguishing feature of the Raman spectra for geological calcite. The fluorescence might originate from mineral-bound or atmosphere-derived organic molecules (Stipp and Hochella 1991), and from certain metal ions occluded within the mineral structure (Mason and Mariano 1990). With the inherent fluorescence of natural calcite, the spectral data derived from confocal Raman microscopy (CRM) require baseline correction, and the isolated residuals are applied to localize fluorophores. To minimize the contributions from instrumental noise, a PCA-guided data denoising algorithm is applied to the baseline-corrected spectral datasets (Fig. S3).

First, we consider the location-averaged Raman spectrum of the rock specimen. The data in **Fig. 1** show peaks at 725 and 1091 $cm^{-1}$ representing the $\nu_4$ (in-plane bending) and $\nu_1$ (symmetric stretching) internal modes of carbonate species, respectively. In relation, the Raman spectrum of pristine calcite exhibit corresponding peaks at 713 and 1085 $cm^{-1}$ (Gunasekaran et al. 2006). An explanation for the observed Raman shifts is the substitution of $Ca^{2+}$ ions by $Mg^{2+}$ ions in the calcite lattice (Borromeo et al. 2017). Considering the progressive increase in Raman shifts with higher $Mg^{2+}$ ion contents of calcite crystals (Borromeo et al. 2017), the $MgCO_3$ content within the rock specimens is estimated at approximately 20 mol%. This clearly shows the enrichment of $Mg^{2+}$ ions within the calcite lattice in rock materials, with implications toward calcite/fluid interfacial energy and wettability alterations of minerals by the incorporation of divalent cations (Sakuma et al. 2014; Andersson et al. 2016). Representing the organic modifications of reservoir minerals, the location-averaged Raman spectrum shows the presence of graphitic hydrocarbons such as asphaltenes and kerogens (Abdallah and Yang 2012; Alabi et al. 2015). Shown in Fig. 1b, the G band (1580 $cm^{-1}$) represents the stretching vibrations of $sp^2$ bonded carbon within aromatic structures, and the D1 band (1351 $cm^{-1}$) indicates in-plane defects or substitutions, which distort the vibrational modes of $sp^2$ carbons (Jawhari et al. 1995; Kelemen and Fang 2001).

The Raman maps for calcite, alongside the distributions of PAHs and fluorescence are shown in Figs. 1c through 1e. At the microscale, the calcite maps present a granular texture, representative of mineral grains. Such structures were also observed by SEM for reservoir carbonates (Cantrell and Hagerty 1999). Here, we additionally observe the colocalization of the spatial distributions of PAHs and fluorescence with calcite grains. Because the core specimens were solvent cleaned before characterization with CRM, the persistence of organic species indicates either high binding affinities of certain PAHs to rock surfaces or the incorporation of hydrocarbons within the mineral structure. The colocalization of PAHs and fluorescence confirms the presence of aromatic molecules as mineral-bound species (Strausz et al. 2009). Such PAHs might constitute wettability-determining organic layers on carbonate surfaces obtained from reservoirs, as also indicated by electron energy-loss spectroscopy and microcomputed tomography (Ivanova et al. 2019a, 2019b).

In all, the Raman analyses show substantial inorganic and organic modifications of reservoir carbonates. Key features are the cationic substitution with $Mg^{2+}$ ions and the presence of PAHs as mineral-bound organic matter. These petrochemical features of reservoir minerals, established by diagenetic processes, also might consequently affect the efficacy of IOR processes. To understand the fluid interactions and temperature dependence that produce such mineral modifications in reservoir conditions, the effects of pertinent fluids such as FW, eqFW, and eqCRO on calcite crystals aged at different temperatures are further investigated.

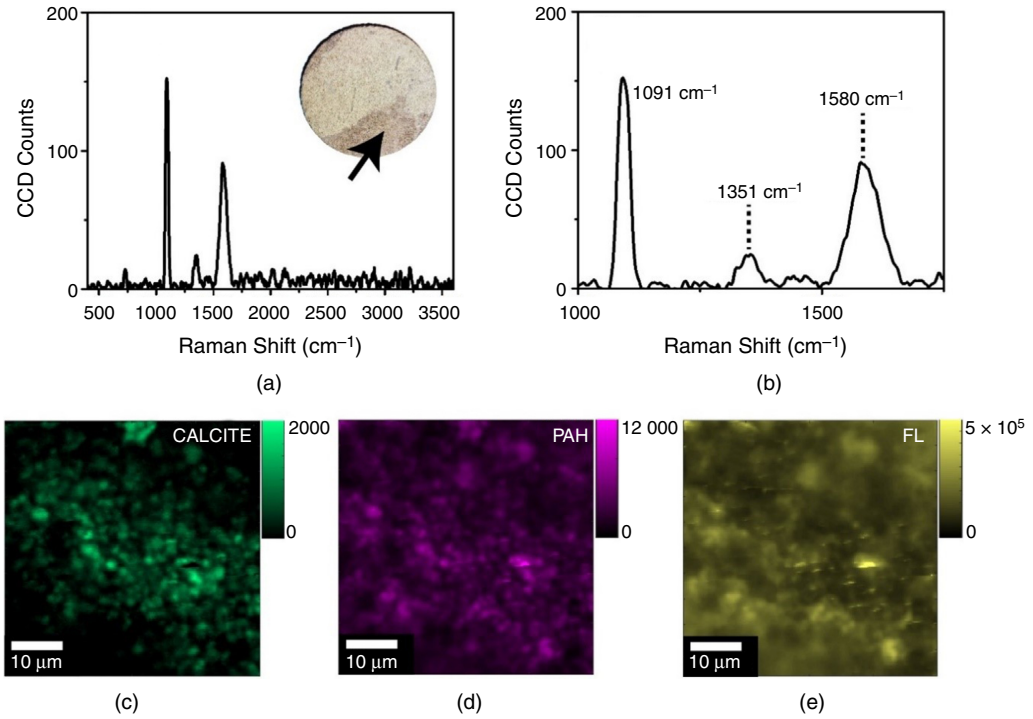


**Fig. 1—(a, b) Representative baseline-corrected spectra of core specimen with peaks specific to Raman active modes of calcite ($v_1$, 1091 $cm^{-1}$) and PAHs (D1, 1351 $cm^{-1}$ as well as G and D2, 1580 $cm^{-1}$). Inset of (a) shows image of core specimen with mapped region (arrow). CRM-derived *x-y* false color images representing distributions of (c) calcite, (d) PAHs, and (e) fluorescence (FL) for the core specimen mapped with a resolution of 200 × 200 pixels. Scale bars represent 10 µm.**

**Inorganic Modifications of Calcite in FW.** Within petroleum reservoirs, rock structures are invariably associated with aqueous fluids termed as "connate water," "interstitial water," or "FW." Serving as the medium for mineral diagenesis, connate waters are typically enriched with diverse ionic species such as $Na^+$, $Ca^{2+}$, $Mg^{2+}$, $Cl^-$, $HCO_3^-$, and $SO_4^{2-}$ in (metastable) equilibrium with mineral phases, while organic species extracted from CRO are also present (Helgeson et al. 1993; Eftekhardadkhah et al. 2016; Rao et al. 2020). To elucidate the inorganic modifications of carbonates by connate waters, Iceland spar crystals were aged in synthetic FW at either RT, 60°C, or 95°C for 16 hours. Evident from SEM micrographs, the FW exposure produces considerable surface reconstruction of calcite in a temperature-dependent manner **(Figs. 2a and 2b).** The surface asperities represent mineral deposition at elevated temperatures, which originates from the combined effects of the retrograde solubility of reservoir pertinent minerals such as anhydrite and calcite (Fig. S4; Plummer and Busenberg 1982; Dai et al. 2017) as well as the rich ionic composition of FW (Table 1). Such topographical modifications are likely to influence mineral wettability, considering that surface roughness can singly affect contact angles estimated in oil/brine/calcite systems (Rao et al. 2020; Sari et al. 2020).

After aging the calcite crystals in FW, the temperature dependence of emergent mineral topography is assessed by AFM. As shown in Figs. 2c through 2e, the surfaces of aged calcite present asperities, with increased prevalence and size for higher aging temperatures. The corresponding height profiles indicate pronounced surface roughness for crystals aged at 95°C, characterized by micro- and nanoscale features atypical of unaged calcite (Fig. S5). Such granular textures can emerge from conditions wherein crystal growth is influenced by ionic "impurity" species such as $Mg^{2+}$ and $SO_4^{2-}$ or occurs via the attachment and crystallization of amorphous particles according to the pathways of nonclassical crystallization (Vavouraki et al. 2008; Rodriguez-Navarro et al. 2016; Xu et al. 2016; Huang et al. 2018). These topographical developments are consistent with corresponding scanning electron micrographs (Fig. S6), wherein crystals aged at 95°C present significant alterations relative to those aged at either 60°C or RT. In addition, the calcite crystals aged at RT exhibit some evidence of surface etching (arrow, Fig. S6). Given the average geothermal gradients of approximately 25 to 30°C/km for Earth's depth, temperature emerges as a key determinant for the surface reconstruction of minerals within reservoirs.

To evaluate the extent of surface reconstruction under different thermal conditions, calcite crystals are partially protected by cured polydimethylsiloxane films as a sacrificial template during the aging procedure (Fig. S7). After removal of the template, height maps are acquired across the protected and exposed calcite surfaces **(Fig. 3).** The offsets in the height profiles are representative of either dissolution or growth of mineral substrates on exposure to FW at different temperatures (Fig. 3d). For crystals aged at RT, the $\Delta z$ values are negative and indicate the dissolution of calcite crystals equivalent to a layer thickness of approximately 20 to 55 nm. On the other hand, aging at either 60 or 95°C produces positive values of $\Delta z$, which correspond to mineral growth with thickness values in the ranges of 100 to 150 nm and 110 to 650 nm, respectively. Overall, the qualitative trend of prominent mineral growth with elevated aging temperature is consistent with the inverse temperature dependence of the thermodynamic solubility of reservoir minerals, such as calcite and anhydrite (Fig. S4). For crystals aged at 95°C, large variations in the thickness of mineral layers are observed (Fig. 3d), which can originate from the dependence of crystal dissolution and growth rates on the distributions of steps, kinks, and etch pits (Arvidson et al. 2003). For instance, even within the same experiment, the growth velocities of steps on calcite surfaces show considerable variations (Astilleros et al. 2010). Such local variations might also apply for crystals aged in FW, wherein a high driving force for crystal growth emerges at elevated temperatures. At high temperatures, the depletion of ion species available for mineral growth can kinetically limit precipitation reactions.

Elemental compositions of FW-aged calcite crystals reveal the incorporation of $Mg^{2+}$ ions into the calcite lattice, which presents a positive correlation with aging temperature (Fig. S8). This relation is consistent with previous studies on calcite overgrowth in simple brines and artificial seawater environments (Lopez et al. 2009). Applying a reservoir related brine composition (FW), the degree of cationic substitution is estimated at approximately 1 and 9 mol% of incorporated $MgCO_3$ contents at 60 and 95°C, respectively (Fig. S8).

The hydrothermal replacement of calcite by magnesium carbonate has been reported in the presence of high $MgCl_2$ contents (1 M) at elevated temperature (200°C) and pressure (Jonas et al. 2015). Here we show that the deposition of Mg-calcite onto calcite substrates also occurs with nominal $Mg^{2+}$ ion contents (~ 90 mM) at lower temperature (60°C) and pressure conditions. With the incorporation of $Mg^{2+}$ ions in the natural carbonates (Fig. 1) as well as FW-aged Iceland spar (Fig. S8), reservoir pertinent mineral surfaces have distinct chemical compositions relative to the typically used synthetic calcite and Iceland spar. Thus, diagenetic reactions concerning carbonates can be moderately replicated at the laboratory scale, supported by the incorporation of ionic impurities into crystal lattices as a function of temperature. Such surface reconstruction events involving the incorporation of "impurity" ions also have key implications for aging procedures routinely used in coreflooding experiments (Anderson 1986).

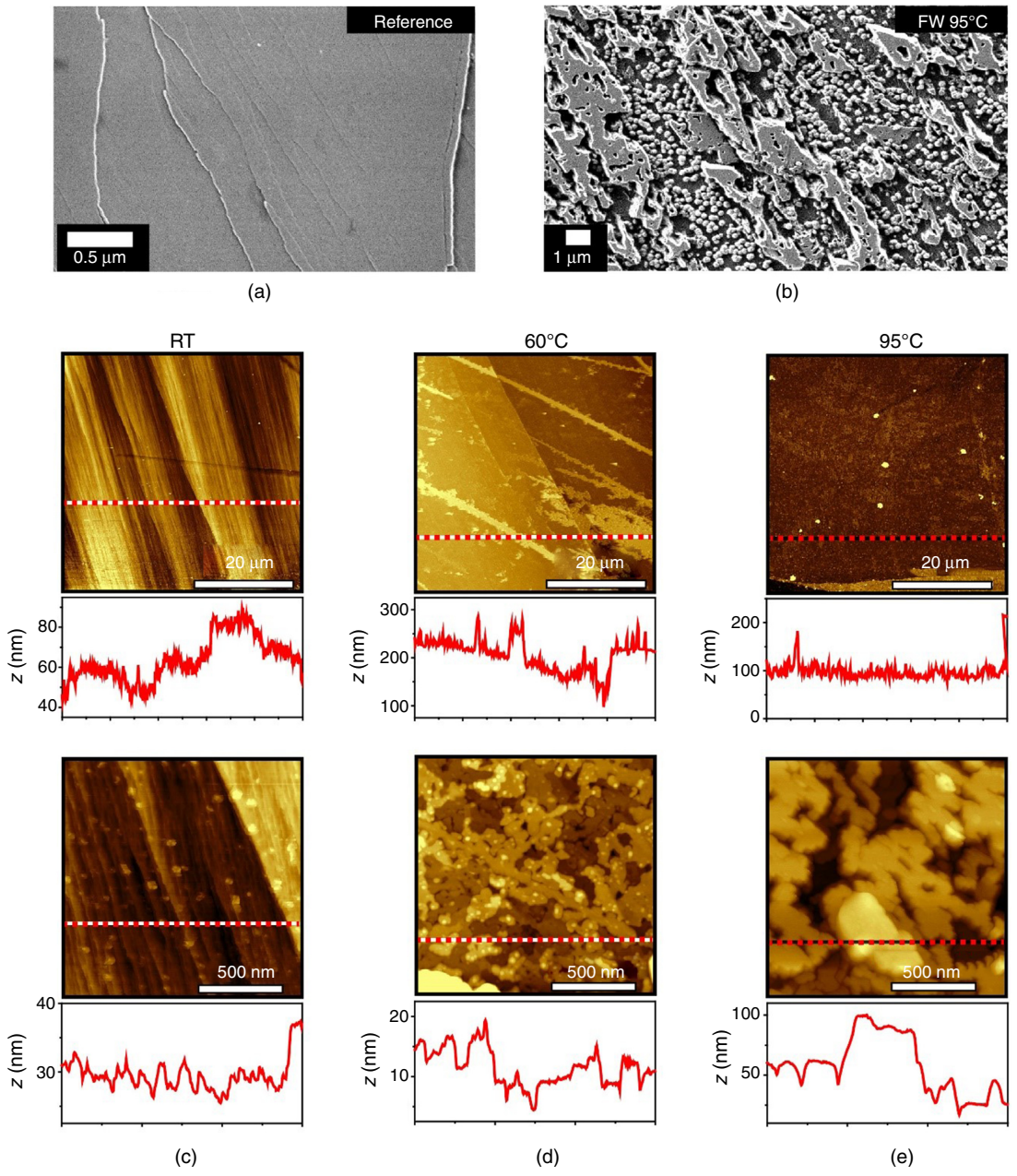


**Fig. 2—Representative scanning electron micrographs of (a) reference calcite and (b) after aging in FW at 95°C for 16 hours. Scale bars represent (a) 0.5 µm and (b) 1 µm. AFM height maps of calcite surfaces after aging in FW at (c) RT, (d) 60°C, and (e) 95°C, at scan areas of 50 × 50 µm and 1.5 × 1.5 µm. Lower panels represent height profiles across the dotted red lines.**

**Organic and Inorganic Modifications of Calcite: Equilibrated FW.** Within reservoirs, interstitial fluids serve as "reaction media" for diagenetic reactions and IOR processes. Given the water solubility of certain CRO components (Shiu et al. 1990), reservoir pertinent aqueous fluids cannot be solely considered as brines with some pure ion compositions. In laboratory studies, one approach for preparing reservoir representative brine and oil compositions is the equilibration of FW and CRO at elevated temperatures for prolonged periods (Eftekhardadkhah et al. 2016; Rao et al. 2020). During equilibration, the transfer of diverse organic molecules such as short-chain alkanes, aromatic, and heterocyclic hydrocarbons from CRO to the formation brine occurs. Using reservoir mimetic equilibrated fluids (i.e., eqFW and eqCRO), we explore the parameter space for the inorganic and organic modifications of carbonates in relation to aging temperature.

The aged crystals were characterized by CRM and fluorescence confocal scanning laser microscope using depth profiling approaches. As shown in **Fig. 4,** the location-averaged Raman spectrum of eqFW- and eqCRO-aged calcite crystals indicate the

presence of graphitic hydrocarbons, with spectral signatures for G (1570 $cm^{-1}$) and D1 (1355 $cm^{-1}$) bands. Using CRM, large area scans in the *x*-*z* plane (i.e., perpendicular to the calcite/air interface) were used to estimate intensity profiles of components as a function of depth (**Fig. 5;** Fig. S9). With increasing aging temperature, the depth profiles show prominent accumulation of polyaromatic and fluorescent molecules at the calcite/air interface for eqFW-aged samples. Although the reference Iceland spar presents some intrinsic fluorescence, the surface deposition of fluorophores from eqFW clearly produces augmented fluorescence for crystals aged at 60 and 95°C. Thus, certain aromatic molecules and fluorophores in eqFW display high affinities to mineral boundaries, with enhanced deposition at elevated temperatures.

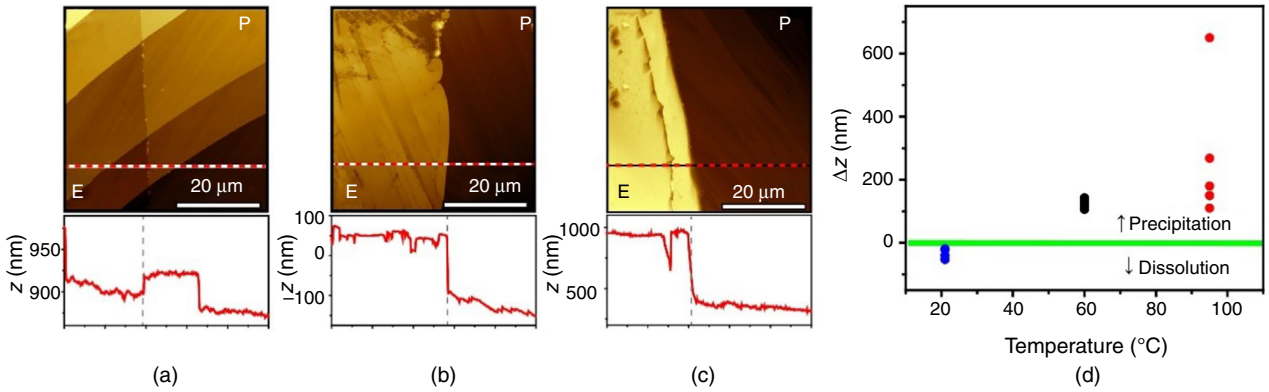


**Fig. 3—AFM height maps across exposed (E) and polydimethylsiloxane protected (P) regions for Iceland spar aged at (a) RT, (b) 60°C, and (c) 95°C for 16 hours in FW, at scan areas of 50 × 50 μm. Lower panels represent height profiles across the dotted red lines; and (d) scatter plot for height changes (Δ*z*) of FW-aged calcite surfaces at different temperatures. Mineral dissolution and growth are indicated by negative and positive Δ*z* values, respectively.**

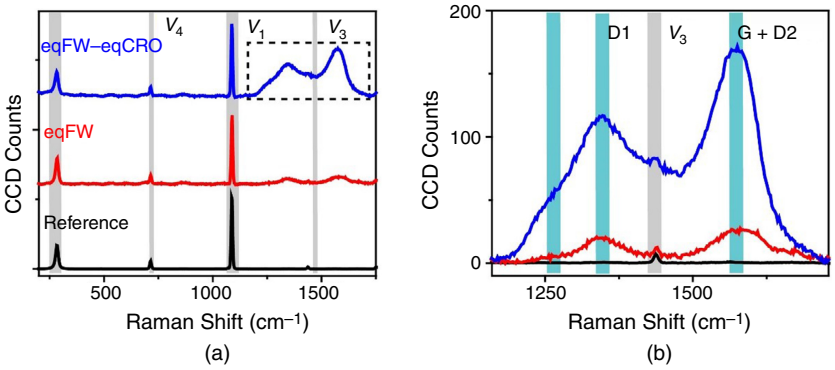


**Fig. 4—(a, b) Representative baseline-corrected spectra of bare calcite (black), eqFW (red), and eqCRO (blue)-treated (95°C) Iceland spar, with peaks specific to Raman active modes of calcite [gray regions, $\nu_4$ (713 $cm^{-1}$), $\nu_1$ (1085 $cm^{-1}$), and $\nu_3$ (1434 $cm^{-1}$)]; and (b) peaks corresponding to organic species (cyan regions) represent D1 (1355 $cm^{-1}$) as well as G and D2 (1570 $cm^{-1}$) bands for PAHs, and a shoulder at ~ 1260 $cm^{-1}$, representing $CH_2$-related vibrations (after Rao et al. 2020).**

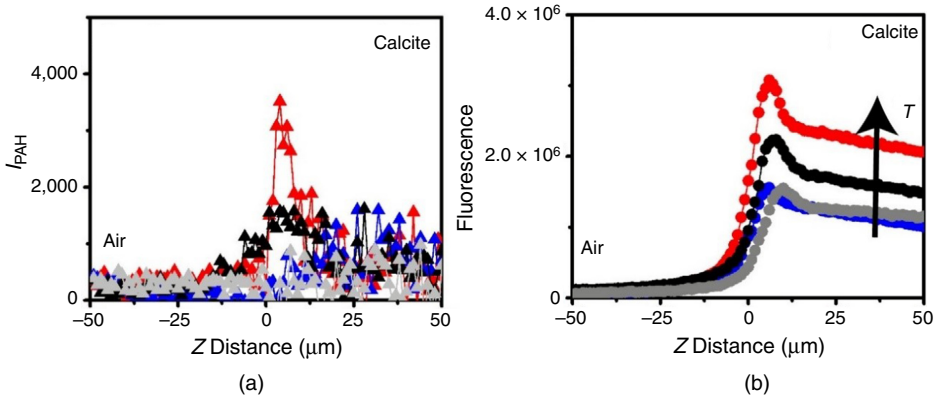


**Fig. 5—Intensity profiles of (a) PAHs (CCD counts) and (b) fluorescence (rel.) across air/calcite interfaces (at Z distance of 0 μm) as functions of depth within the sample, for eqFW-aged treated at RT (blue), 60°C (black), and 95°C (red). Corresponding plots for reference calcite are indicated (gray).**

Additional CSLM-derived fluorescence depth profiles taken at various *x*-*y* locations indicate that the lateral distributions of fluorophores on the aged mineral substrates are nonuniform (Fig. S10). An explanation might be the preferential deposition of CRO-derived water-soluble organic species onto high-energy surface features such as macrosteps that separate relatively flat crystalline surfaces (Rao et al. 2020). Specific interactions of organic molecules such as amino acids and peptides with step edges on crystalline surfaces have been reported elsewhere (Orme et al. 2001; Elhadj et al. 2006). Related organo-mineral interactions can produce substantial heterogeneity for the surface modification of carbonates. Interestingly, fluorophores are also associated with mineral grains in the natural counterpart obtained from an oil reservoir (Fig. 1).

Organic species constituting eqFW can regulate the inorganic modifications of calcite driven by conditions of supersaturation at elevated temperatures (Fig. 3). Previous studies show that, upon thermal treatment, precipitates formed in eqFW present Raman spectral features for amorphous calcium carbonate particles with coassociated $SO_4^{2-}$ species, whereas, for particles similarly derived from unaged FW, the Raman characterization only yields the spectral signature of amorphous calcium carbonate (Rao et al. 2020). Evident from the representative Raman spectra of eqFW-aged calcite (**Fig. 6;** Table S2), we further show that the interactions between organic species and crystal precursors might govern the extent of cationic substituent of lattice $Ca^{2+}$ ions by $Mg^{2+}$ ions. Raman shifts for the $\nu_1$ (in-plane bending) internal modes of carbonate from 1084 to approximately 1087 $cm^{-1}$ are observed for Iceland spar crystals aged at 95°C. This shift corresponds to $MgCO_3$ contents of approximately 5 mol% (Borromeo et al. 2017), which is lower than the values estimated (~ 9 mol%) for FW-aged crystals by energy-dispersive X-ray spectroscopy (Fig. S8). The incorporation of $Mg^{2+}$ ions in the crystal structure might be suppressed by the complexation of $Mg^{2+}$ ions by polar organic molecules as relatively stable complexes. This can restrict the net free ion contents accessible for cationic substitution reactions at mineral surfaces. In addition, the organic deposits on the calcite surface might also limit diffusive transport and kinetically inhibit cation substitution. Although identifying the precise mechanism(s) by which CRO-derived organic molecules control inorganic modifications of minerals is beyond the scope of this study, the regulation of reactions, such as cation substitution and dolomitization by solute- and surface-bound organic species, emerges crucial, in addition to the established parameters of temperature, surface area, and saturation index (Arvidson and Mackenzie 1999; Jonas et al. 2015).

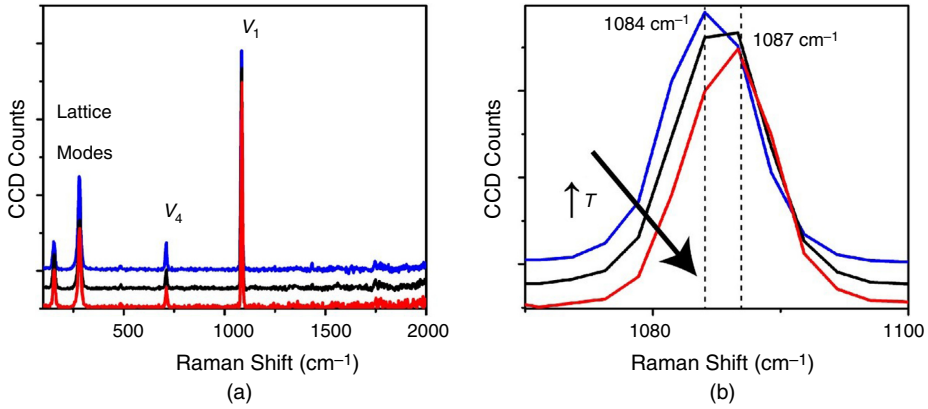


**Fig. 6—(a) Representative baseline-corrected spectra of Iceland spar aged in eqFW at RT (blue), 60°C (black), and 95°C (red) with peaks specific to calcite; and (b) aging temperature-dependent Raman shifts in the $\nu_1$ symmetric mode (Table S2).**

**Organic Modifications of Calcite: Equilibrated CRO.** Studies addressing the wettability alteration of model calcite substrates via CRO contact identify exposure periods and temperature as key parameters determining "oil-wet" responses (Hirasaki and Zhang 2004). To investigate the temperature dependence of underlying microscopic reactions, eqFW-preconditioned calcite crystals were aged in eqCRO for an extended period at either RT, 60°C, or 95°C (Fig. S1). As depicted in **Fig. 7,** SEM images of eqCRO-treated crystals aged at either RT or 95°C are distinct from the reference calcite (Fig. 2) and indicate substantial organic modifications of the mineral phase. On aging at 95°C, deposition of an organic layer is evident (arrow, Fig. 7b), which is sufficiently thick to obscure distinctive features of the crystalline substrate. The elemental composition of these organic adlayers is enriched in carbon, as shown by energy-dispersive X-ray spectroscopy (Fig. S11). These surface modifications induced at elevated temperatures are also shown by optical micrographs of eqFW- and eqCRO-aged calcite (Fig. S12).

AFM is further used to characterize the micro- and nanoscale topographical features of calcite resultant of prolonged contact with eqCRO (Fig. 7). Consistent with the scanning electron micrographs, the prominent deposition of PAH-enriched organic particles from eqCRO at 95°C envelope the mineral surfaces (Fig. 7e). The aged substrates present surface features with lateral dimensions in the range of approximately 10 nm to 5 µm. Exhibiting G and the D1 Raman bands characteristic of graphitic hydrocarbons (Fig. 4), the particle deposits appear primarily composed of PAHs such as asphaltenes (Abdallah and Yang 2012; Alabi et al. 2015). Some studies have suggested asphaltenes as major components of the deposited material on oil-exposed surfaces, with indications for strong adsorption in the presence of extracted asphaltenes (González and Moreira 1991; Piro et al. 1996; Kumar et al. 2005). Here we show the direct deposition of PAH-rich aggregates from eqCRO on mineral surfaces, and also identify a positive correlation with aging temperature.

Shown in **Figs. 8** and S13, the calcite substrates are characterized by CRM following a depth profiling approach. Following a similar trend as for eqFW-aged crystals, an enhanced deposition of polyaromatic and fluorescent molecules at the calcite/air interface positively correlates with aging temperature. After eqCRO treatment at 95°C, the intensity value of the PAH component at the calcite surface is about twofold that of the corresponding eqFW-aged specimen (Fig. 8). Additionally, shown in *x*-*y* distribution maps, sites of mineral reconstruction such as macrosteps accumulate polyaromatic and fluorescent components (arrows, Fig. S14). Thus, reactions of mineral dissolution-precipitation (i.e., small local variations in ionic conditions) can explain the heterogeneous deposition of polyaromatic molecules from reservoir related fluids (eqFW and eqCRO) onto mineral surfaces.

Here it is important to note that the Raman signal is proportional to the abundance of scattering molecules as well as the scattering cross section. This might produce high relative sensitivities (intrinsic bias) toward conjugated molecules (Wood et al. 2017), thereby obscuring the detection of less abundant or smaller (e.g., aliphatic) molecules. For instance, in comparison to the predominant deposition of PAHs on carbonates shown in the present study, solid-state nuclear magnetic resonance spectroscopy identifies alkyl and acidic

groups adsorbed onto calcite in CRO environments (Sørgård et al. 2017). Part of this discrepancy might also be attributed to the cleaning of the CRO-treated samples, using solvents such as toluene and decane before analytical characterization. Such solvents might selectively extract or precipitate certain organic molecules (Kumar et al. 2005; Subramanian et al. 2017). In addition, the notion that molecules other than PAHs get deposited on calcite is also supported by the rich composition of CRO containing several thousands of chemical entities (Beens et al. 2000; Marshall and Rodgers 2008). This makes it likely that synergistic interactions between acidic, aliphatic, and aromatic groups occur in the organic modification of carbonate surfaces. For instance, from FTIR, the calcite-binding organic molecules from eqFW and eqCRO are also shown to contain polar moieties (Rao et al. 2020), which can support acid-base or ion-bridging interactions with surface species of carbonates.

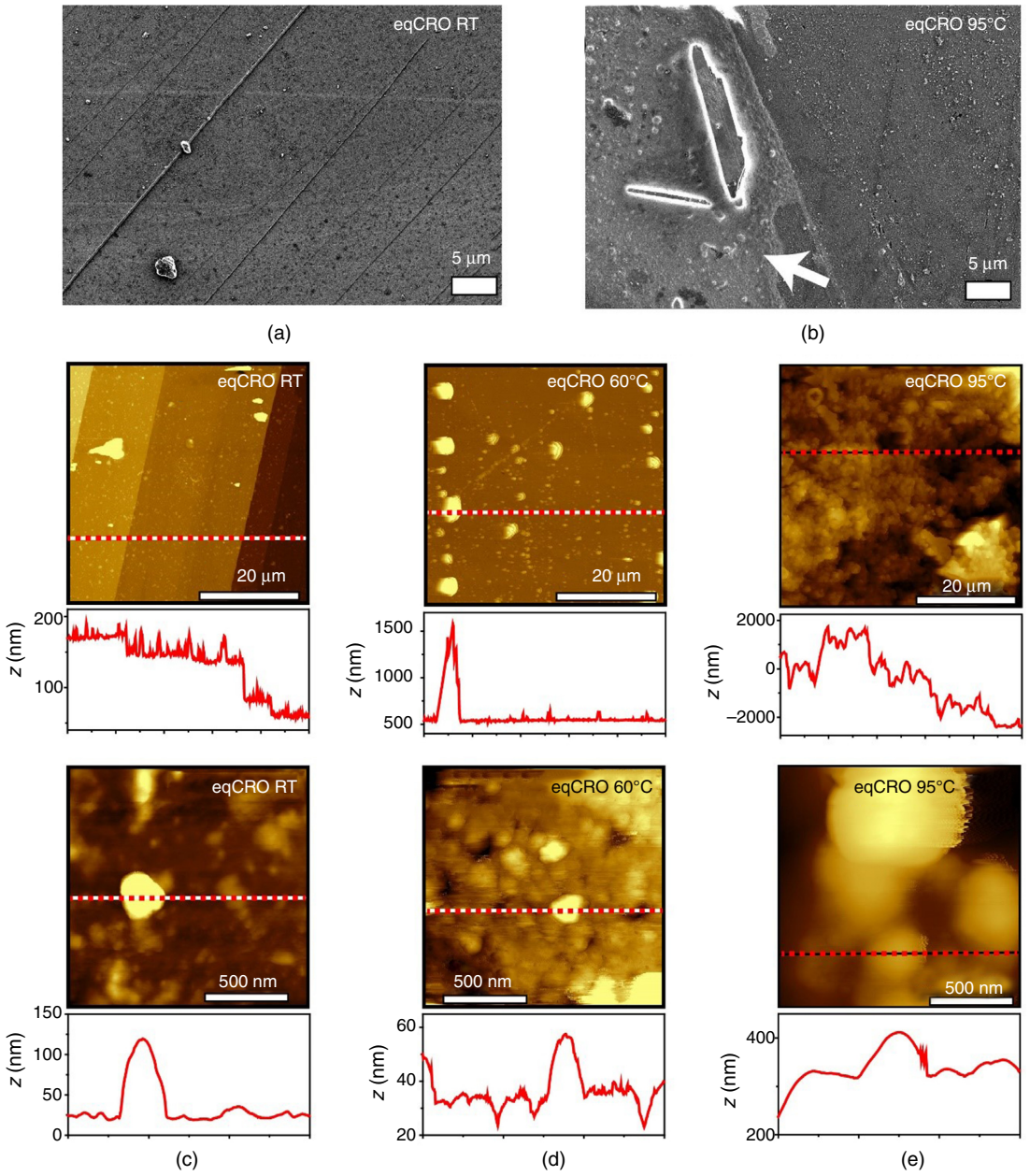


**Fig. 7—Representative scanning electron micrographs of reference Iceland spar treated with eqCRO at (a) RT and (b) 95°C. Scale bars represent 5 µm. AFM height maps of surfaces in air for Iceland spar after aging in eqCRO at (c) RT, (d) 60°C, and (e) 95°C, at scan areas of 50 × 50 µm and 1.5 × 1.5 µm. Lower panels represent height profiles across the dotted red lines.**

A key result of this study identifies temperature as an important parameter for the organic modifications of calcite with PAHs in reservoir pertinent brines and CRO. Previous investigations on the adsorption of organic molecules from CRO onto calcite crystals have primarily focused on aliphatic acids and polyaromatic molecules. Long-chain fatty acids ($\geq C_8$) exhibit relatively high affinities for carbonate surfaces, resulting in apparent oil-wet characteristics (Thomas et al. 1993a). Bonding to the surface $Ca^{2+}$ ions via carboxyl groups, the adsorption density of fatty acids decreases at high temperatures due to the prograde solubility of corresponding organo-calcium salts (Young and Miller 2000). However, the notion of aliphatic acids as surface modifiers at high temperatures within reservoirs cannot be disqualified, due to complex-salinity-dependent sorption behaviors involving solute complexes and micelles (Lahann and Campbell 1980) as well as the high $Ca^{2+}$ ion contents of connate waters, which can suppress the solubilization of organic salts. Moreover, analytical characterizations of reservoir rocks show that organic layers are bonded with calcite via Ca–O bonds of certain organic acids (Ivanova et al. 2019a, 2019b).

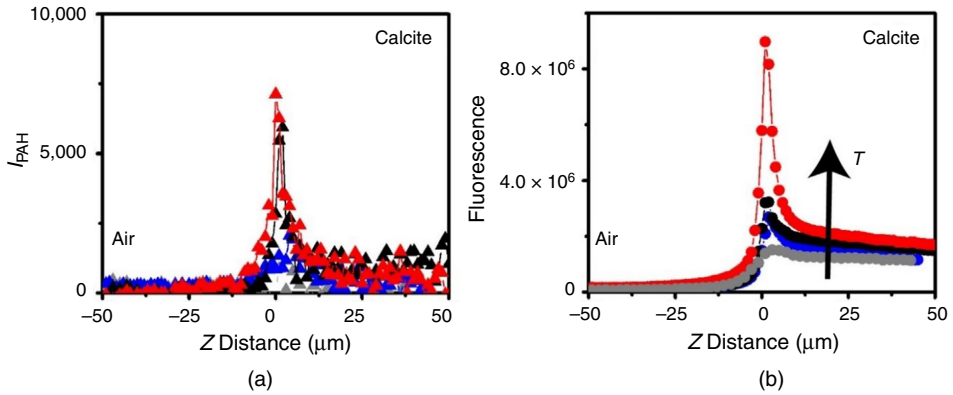


**Fig. 8—Intensity profiles of (a) PAHs (CCD counts) and (b) fluorescence (rel.) across air/calcite interfaces (at Z distance of approximately 0 μm) as functions of depth within the sample, for eqCRO-aged calcite treated at RT (blue), 60°C (black), and 95°C (red). Corresponding profiles for reference calcite are indicated (gray).**

Although the deposition of PAHs onto calcite surfaces from CRO is evident in the present study, the mechanisms for the sorption of polyaromatic molecules are not well understood. Considering their significant fraction in CRO (approximately 2.8% mass; Table S1), asphaltenes should play an important role. Indeed, their adsorption on Iceland spar and reservoir carbonates from toluene solutions has been demonstrated, with some dependence on the chemistry of thin brine films (Piro et al. 1996; Saraji et al. 2013). Reported values of surface coverage by asphaltenes deposited from toluene solutions are approximately 0.45 mg/g for carbonates and as high as 20 mg/g for silica (Piro et al. 1996; Acevedo et al. 2000). This indicates continuous or multilayer type of adsorption, consistent with the height maps of eqCRO-aged calcite crystals that exhibit organic aggregates in range of approximately 10 nm to 5 μm (Fig. 7). The observed resilience of the PAH particles toward toluene washing is also consistent with previous reports for asphaltenes adsorbed on carbonates (Piro et al. 1996). With these similarities, it is reasonable to discuss the physical basis for increased deposition of the PAH-enriched particles at elevated temperatures, primarily in the context of asphaltenic compositions.

The thermal dependence of organic modifications of carbonates can be explained in view of the aggregation dynamics of asphaltenes and the fundamental nature of sorption processes on a soluble substrate such as calcite. First, temperature-induced asphaltene precipitation encompasses multiple factors such as molecular solubility, compositional changes of dispersion media, and variations in diffusivity (Hirschberg et al. 1984; Maqbool et al. 2011). At elevated temperatures, the onset of precipitation is shorter, and asphaltene microparticles are produced via the colloidal destabilization and coalescence of smaller aggregates (Maqbool et al. 2011). Second, for the sorption of ionic or polymeric species onto calcite, surface precipitation models are more applicable relative to monolayer adsorption models (Comans and Middelburg 1987; Cabane et al. 1997). Cations released upon calcite dissolution can form complexes with adsorbents, thereby influencing their solubility and sorption behavior. For instance, initial complexation events in bulk fluid and subsequent surface precipitation of $Ca^{2+}$-polyelectrolyte complexes underlay the surface modification of calcium carbonate by polyacrylic acid (Cabane et al. 1997). Such interactions might also apply for certain subfractions of the molecular ensemble of asphaltenes with polar modifications. In support of this notion, irreversibly bound asphaltenes (isolated by dissolution of calcite substrates) present higher contents of carbonyl or carboxylic groups and are aggregation prone in toluene (Subramanian et al. 2017). By considering both these factors, the colloidal destabilization of PAH aggregates at high temperature, and the surface precipitation model for carbonates, our observations of the temperature-driven surface enrichment of organic particles, can be explained. The proposed mechanism involves the surface precipitation of PAHs with polar modifications and ionic species, as organo-calcium salts on carbonates. Based on the surface precipitation model (Comans and Middelburg 1987; Cabane et al. 1997), key chemical equilibria include:

a. Dissolution/precipitation of carbonates (related to solubility product of the mineral substrate, $Ksp_{\text{calcite}}$)

$$CaCO_{3(s)} + > CaCO_3^{\circ} + H^+ \rightleftarrows > CaCO_3^{\circ} + Ca^{2+} + HCO_3^-. \quad \ldots\ldots (1)$$

b. Dissolution/precipitation of organo-calcium salts as a surface phase (related to solubility product of the surface phase, $Ksp_{\text{organo-calcium}}$)

$$> CaCO_3^{\circ} + Ca^{2+} + 2RCOOH \rightleftarrows CaCO_{3(s)} + > Ca(RCOO)_2 + 2H^+. \quad \ldots\ldots (2)$$

This mechanism is supported, first, from the resilience of PAH deposits toward dissolution in toluene, which is indicative of certain polar constituents. Second, sites of mineral reconstruction such as steps accumulate more PAHs (Fig. S14), where dissolution rates (i.e., local $Ca^{2+}$ contents) are significantly higher than those of crystal faces (Noiriel et al. 2019). In oil/brine/mineral systems, the phase transfer of acids from CRO to brines and their deprotonation also occurs (Rao et al. 2020), represented by:

$$RCOOH_{oil} \rightleftarrows RCOO^-{}_{brine} + H^+{}_{brine}. \quad \ldots\ldots (3)$$

Further studies are required to address the intricate interplay between these coupled chemical reactions (Eqs. 1 through 3) involving metallo-organic complexes.

**Mineral Wettability.** We now consider the influence of the temperature of aging (first in eqFW, then in eqCRO) on the wettability of the modified calcite substrates. This relation is studied by measuring the dynamic contact angles of CRO droplets in captive bubble geometry, using eqFW at RT as the ambient. Dynamic contact angles are preferred over static ones because on inhomogeneous substrates, the contact angle can adopt any value between a minimum receding ($\theta^{\text{rec}}$) angle and a maximum advancing ($\theta^{\text{adv}}$) angle. As shown in Figs. 7 and S14, our Iceland spar substrates show both substantial chemical and topographical heterogeneity. For our CRO droplets, only the oil-advancing (brine-receding) contact angles could be reliably measured. Receding oil contact angles could not be measured accurately but fall well below 20°. Both the large contact-angle hysteresis ($\theta^{\text{adv}}_{\text{brine}} - \theta^{\text{rec}}_{\text{brine}}$) and the broad distributions of $\theta^{\text{rec}}_{\text{brine}}$ indicate a strong surface heterogeneity of the calcite, in particular after CRO aging.

Freshly cleaved Iceland spar (reference, unaged calcite) substrates produce $\theta^{rec}_{brine}$ values between 44° and 68°, representative of moderate hydrophilicity. On the other hand, for calcite surfaces aged in eqCRO at 95°C, a broad distribution of $\theta^{rec}_{brine}$ values from approximately 42 to 129° is observed. This indicates an "intermediate-wet" or "oil-wet" nature, which emerges from the "artificial diagenesis" treatment with eqCRO. In relation, for calcite surfaces, initially aged in eqCRO at RT, the $\theta^{rec}_{brine}$ values are in the range of approximately 36° and 70°, similar to those of unaged Iceland spar. These observations reveal a clear correlation between aging temperature applied during eqCRO contact and the resulting wettability of Iceland spar surfaces **(Fig. 9).**

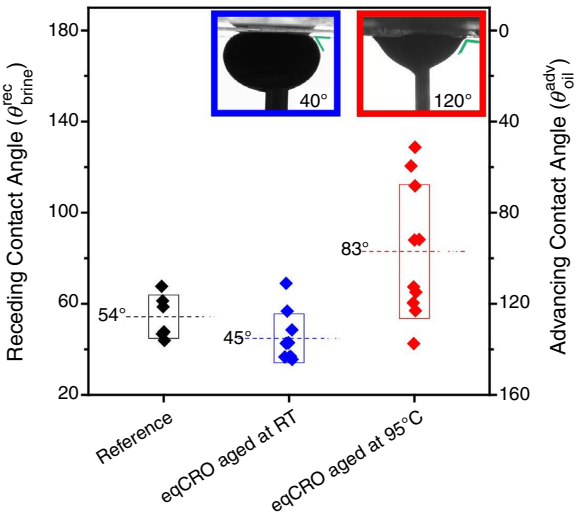


**Fig. 9—Box chart for the distributions of contact angles ($\theta^{rec}_{brine}$ and $\theta^{adv}_{oil}$) for CRO (eqCRO) droplets on Iceland spar substrates, freshly cleaved (reference, black) and also after aging in eqCRO at either RT (blue) or at 95°C (red). Box-splitting horizontal dotted lines represent the mean contact angle while the box range corresponds to ±1 standard deviation. Insets: brine contact angles ($\theta^{rec}_{brine}$) for substrates aged in eqCRO at either RT (left) or 95°C (right).**

Evident from the enhanced deposition of CRO-derived hydrocarbons on calcite surfaces at elevated aging temperatures (Fig. 8), the PAH-enriched adlayer emerges as a key factor that renders the intermediate-wet or oil-wet characteristic of carbonates. Although the exposure of mineral surfaces to CRO at RT produces some deposition of organic particles (Figs. 8 and 9), the observed lack of wettability alteration toward oil-wet likely originates from limited surface coverage by the organic adlayer of the relatively hydrophilic mineral substrate. Given the chemical heterogeneity of PAHs constituting CRO (Marshall and Rodgers 2008; Subramanian et al. 2017), a temperature-dependent partitioning of certain surface-active species between the organic adlayer on mineral surfaces and the bulk brine or oil phase might also apply. In principle, this phenomenon might yield CRO composition-dependent wetting characteristics of organic adlayers deposited on rock surfaces.

**Reactivity Modulated by Organic Adlayers.** Organic adlayers, formed upon contact with eqCRO at elevated temperature, appear to effectively isolate the calcite surfaces from ambient fluids (Fig. 7). Such layers could thus influence the diffusive transport associated with IOR-related mineral/fluid interactions as well as diagenetic reactions such as phase transformations. To examine this scenario, we assessed the dissolution kinetics of precipitated calcite powders, initially aged in FW, eqFW, or eqCRO at 95°C (Fig. S2). The use of synthetic calcite powders eliminates possible interference of intrinsic fluorophores and ionic impurities as are present in Iceland spar. From CRM, distribution maps of calcite and PAH for the reference, FW-aged, and eqFW-aged samples are shown **(Fig. 10a).** Corresponding distributions of PAHs show few enriched regions for eqFW-aged crystals whereas eqCRO-aged crystals display prominent signal from these hydrocarbons. As shown in Fig. S15, FTIR spectroscopy is used to further characterize the calcite powders and bands are assigned in accordance with literature values (Coates 2006). The infrared spectra of eqCRO-aged calcite display bands in the range of 2800 to 3100 $cm^{-1}$, representative of distinct aliphatic and aromatic C-H stretching modes. As summarized in Table S3, the peak positions correspond to symmetrical and asymmetrical C-H stretching, suggestive of CRO-derived aromatic hydrocarbons such as asphaltenes and kerogens (Coelho et al. 2007). Relative organic contents are estimated from the ratio of band intensities for alkyl molecules and calcite [i.e., ($CH_2$ symmetric stretching (2922 $cm^{-1}$) + $CH_3$ symmetric stretching (2953 $cm^{-1}$)/(calcite $\nu_4$, 710 $cm^{-1}$)]. The hydrocarbon fractions associated with calcite powders are significantly enhanced on treatment with eqFW and eqCRO (Fig. 10b). Consistent with results of the Raman characterization (Fig. 8), the eqCRO-aged calcite powders are much more abundant in oil-derived hydrocarbons.

The ability of the organic adlayers to inhibit the calcite dissolution is studied with measurements of $Ca^{2+}$ ion selective potential. Given the high sensitivity to initial contents of the analyte and difficulties in determining the end point in dissolution studies, the Guggenheim approach is used (Hefter and Tomkins 2003). Exemplified in Fig. S16, this approach is used to estimate pseudofirst-order rate constants from the kinetic data of calcite dissolution acquired at 40°C. As shown in Fig. 10c, the eqCRO-derived organic adlayers suppress the dissolution of underlying calcite substrates and produce apparent rate constants of approximately 30% lower than that of pristine calcite powders. For eqFW-aged calcite, the dissolution rates are intermediate and approximately 55% that of the reference powders. On the other hand, the estimated rate constants of FW-aged (remineralized but free of organics) calcite powders do not significantly deviate from those of reference samples. These trends are in agreement with a calcite dissolution inhibiting role of the organic adlayer.

Previous studies demonstrate suppressed calcite dissolution after treatment with strongly adsorbing organic molecules (Thomas et al. 1993b). Thorough coating of crystals with organic molecules is a proposed explanation for inhibited dissolution. Even inorganic complexes, intrinsic to some natural carbonates, can adsorb irreversibly onto mineral surfaces and decrease the rates of mineral dissolution (Eisenlohr et al. 1999). In the present study, the presence of PAH-rich adlayers on the eqCRO-aged surfaces (Figs. 8 and 10)

equally appears to suppress mineral reactivity, possibly related to the diffusion limitation of transport processes at the surfaces. Thus, in addition to mechanistic roles in determining mineral wettability (Chen et al. 2017; Ivanova et al. 2019a; Rao et al. 2020), the organic adlayer serves as a potent diffusive barrier influencing mineral reactivity. During IOR processes, any form of chemical reactivity of the underlying carbonate rock will obviously be affected by these adlayers. In this light, modeling approaches that resort to speciation and rate equations of pristine calcite surfaces alone seem questionable.

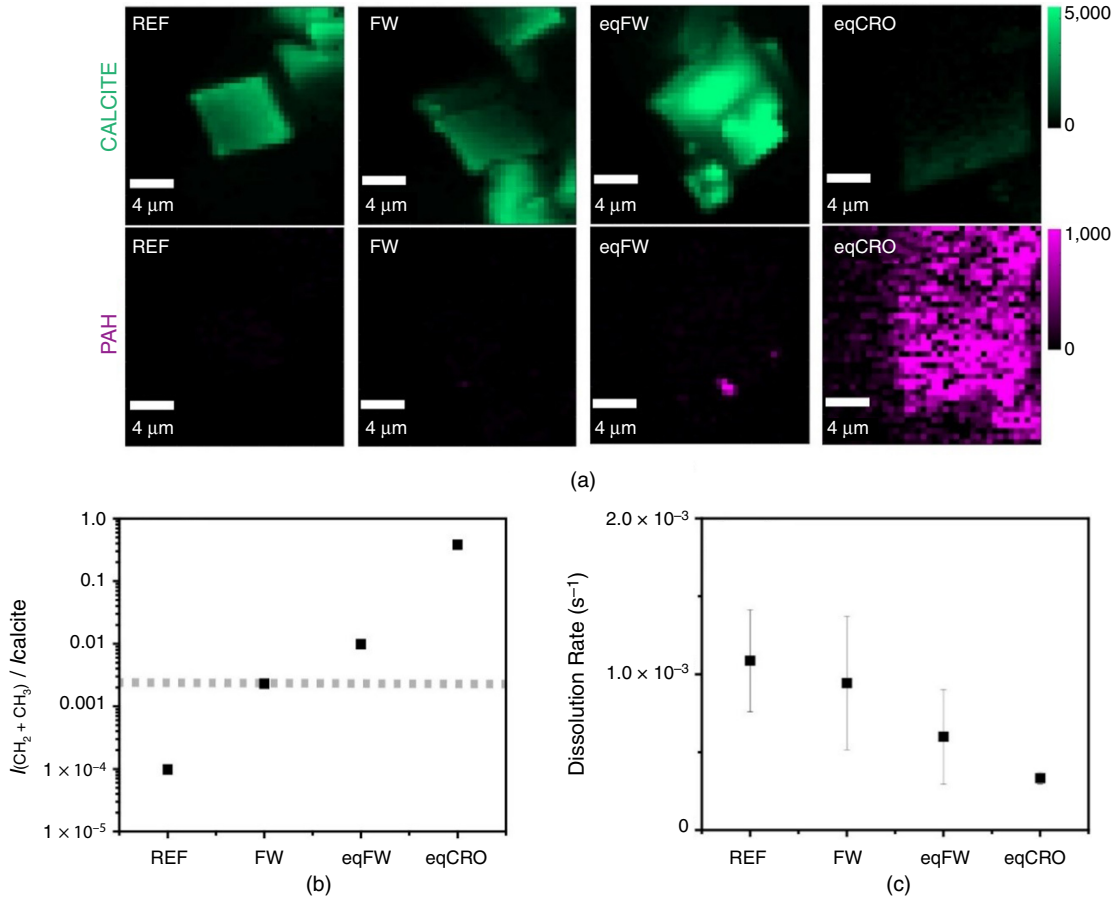


**Fig. 10—(a) CRM-derived *x-y* false color maps representing distributions of calcite (green) and PAHs (purple) for calcite powders aged in different ambient fluids at 95°C. Image resolutions correspond to 40 × 40 pixels. Scale bars represent 4 μm; (b) relative organic contents estimated from the ratio of band intensities for alkyl molecules [sum of $CH_2$ symmetric stretching (2922 $cm^{-1}$) and $CH_3$ symmetric stretching (2953 $cm^{-1}$)] and calcite ($v_4$, 710 $cm^{-1}$) for reference (REF), FW-, eqFW-, and eqCRO-aged specimens. Values below a threshold (dotted line) indicate the absence of coassociated hydrocarbon fractions; and (c) estimated dissolution rates of calcite powders at 40°C.**

**Implications for Oil Recovery.** Results of the "artificial diagenesis" in conjunction with the structural observations of core specimens show that interactions with brines and CRO produce distinct modifications of carbonates within reservoir environments. Deposited from reservoir pertinent brines (FW and eqFW) at elevated temperatures, the mineral overgrowths show the incorporation of $Mg^{2+}$ ions within the calcite lattice. Such cation substitutions can alter the calcite/fluid interfacial energy, possibly enough to impact the macroscopic contact angle. For instance, ions that are hydrated more strongly than $Ca^{2+}$ (such as $Mg^{2+}$) can render calcite more hydrophilic (Andersson et al. 2016). In addition, the solubility of calcite is enhanced on $Mg^{2+}$ incorporation. Surfaces of FW-aged calcite specimens with about ~9% $MgCO_3$ (Fig. S8), present approximately 50% solubility enhancements relative to pristine calcite (Sun et al. 2015). Both these considerations dissuade the use of pristine "unaged" calcite, which is not a true representative of the mineral interfaces within reservoirs.

Primarily determining the oil-wet behavior of aged calcite, polyaromatic molecules emerge as key constituents of the organic deposits from eqCRO. Enhanced PAH deposition resulting in more oil-wet contact angles also elucidates previous observations of CROs with high asphaltene contents producing relatively oil-wet cores after aging (Cuiec 1984). The organic layer also significantly suppresses calcite dissolution, with key implications toward the kinetics of mineralogical reactions, such as cation substitution and dolomitization (Putnis 2009) and of IOR pertinent reactions such as rock dissolution and brine/CRO interactions (Yutkin et al. 2018). With coinciding observations of organic adlayers for natural and reservoir mimetic minerals (Chen et al. 2017; Ivanova et al. 2019b; Rao et al. 2020), addressing the stability, detachment, and mobilization of these organic adlayers in different injection fluid environments might become a key element, which facilitates not only the knowledge of reservoir geochemistry but also the further advancement of IOR strategies.

Our study also elucidates the aging steps applied in coreflooding, which is common test to determine oil recovery rate, residual oil saturation, and relative permeability in reservoir simulating conditions. Core aging generally entails initial saturation steps, first with formation brine and then CRO, followed by extended aging at reservoir pertinent temperatures (Anderson 1986). Key developments in the IOR field have been made via coreflooding experiments (Jadhunandan and Morrow 1995; Yousef et al. 2011; Austad et al. 2012; Jackson et al. 2016). Yet the microscale chemical and topographical transitions brought about by these aging steps are not understood. Addressing this knowledge gap, results of this study can benefit the controlled replication of surface properties in petroleum engineering experiments.

Interestingly, our results show a pronounced deposition of organic particles at elevated temperatures, resulting in relatively more oil-wet surfaces. On the contrary, some studies relate increased aging temperature with less oil-wet carbonate surfaces, attributed to the increased solubility of surface-active molecules (e.g., fatty acids) (Anderson 1986; Thomas et al. 1993b). This contradiction was also noted by Buckley (2001), who considered the influences of temperature on wetting properties of reservoir carbonates as "unresolved." The resolution appears to lay in the fundamental mechanisms of carbonate modification, described by the surface precipitation model (Comans and Middelburg 1987). While considering the surface deposits as organo-calcium salts, the formation and stability of these salts (described by their solubility product, $Ksp_{\text{organo-calcium}}$) depend on local $Ca^{2+}$ ion contents—minimum (nonzero) values of which are set by carbonate dissolution—and organic acid contents in FWs and CRO (reflected in the total acid number). Given the solubility of carbonates (Fig. S4), mineral dissolution introduces higher $Ca^{2+}$ ion contents in ambient brine films, which in turn can locally precipitate organo-calcium salts (Eqs. 1 and 2). This is partly reflected in the local accumulation of PAHs at macrosteps on calcite surfaces (Fig. S14). Whereas the availability of organic acids in CRO and FWs can significantly vary with respect to the source, storage conditions, and also experimental steps such as fluid equilibration and aging timescales (Eq. 3). Against this background, the temperature dependence of the surface precipitation of organo-calcium salts (producing wettability alteration to oil-wet) depends on their respective retrograde or prograde solubilities. In consequence, the heterogeneous composition and variability among the source of CROs can account for the contradictory accounts of the relations between aging temperature and wettability of carbonate surfaces.

Based on this reasoning, we anticipate that the saturation indices of ambient brines with respect to the organo-calcium salts will affect the stability of the organic layers, and thereby contact-angle estimates. This is demonstrated by lower $\theta^{\text{rec}}_{\text{brine}}$ values observed in ambient FW relative to ambient eqFW for eqCRO-aged calcite specimens (Fig. S17). Due to prior equilibration with calcite and CRO, the eqFW contains substantial contents of $Ca^{2+}$ ions and organic species, which can suppress the dissolution of surface organo-calcium salts (Eq. 2). Whereas contact-angle values estimated in the relatively undersaturated FW reflect more "water-wet" characteristics, due to destabilization or detachment of the organo-calcium layer. Such experimental variations (related to aging procedures and wettability estimation) can significantly affect the delicate balance of the coupled chemical equilibria (Eqs. 1 through 3). Thus, method variations also explain the inconsistent reports on the temperature dependence of the wettability of carbonate surfaces, reflected in positive, negative correlations and even nonmonotonic trends (Hjelmeland and Larrondo 1986; Sayyouh et al. 1991; Lu et al. 2017).

## Conclusions

Within reservoirs, mineral/fluid interactions produce distinct chemical and topographical modifications. Shown by the "artificial diagenesis" or "aging" of carbonates, mineral modifications encompass surface reconstruction by dissolution-precipitation reactions, mineral overgrowths containing Mg-calcite, and deposition of PAH-enriched particles as organic adlayers. Each of these processes shows a clear positive correlation with aging temperature. These findings are of relevance for understanding diagenetic alterations of carbonates, which establish mineral-adsorbent/fluid interfaces (setting the initial conditions of IOR) and also guiding the design of more representative experimental approaches.

Separating minerals from ambient fluids, organic layers are an important feature of oil/brine/mineral interfaces within natural and mimetic reservoir environments. The PAH-rich layers envelop relatively hydrophilic mineral surfaces and thereby produce a wettability transition toward an "intermediate-wet" or "oil-wet" nature. The organic layer also acts as a diffusion barrier, with key implications toward the transformation and reactivity of mineral phases (Putnis 2009). This surface chemistry is governed by an interplay between bulk and surface reactions involving ionic and organic species (Eqs. 1 through 3), involving the surface precipitation of organo-calcium salts. Physical consideration of the organic deposits as "organo-inorganic salts" provides new insights for addressing the wettability alterations of carbonate reservoirs. In IOR processes such as low-salinity waterflooding, proposed mechanisms often focus on mineral/brine interactions such as mineral dissolution, double-layer expansion (Lashkarbolooki et al. 2016), and the role of $SO_4^{2-}$ species originating from anhydrite dissolution (Fathi et al. 2011; Austad et al. 2012). However, within this intricate scheme, the enrichment of certain hydrocarbons as wettability determining organic layers has not been systematically addressed. For this, the stability and mobilization of the organic deposits in relation to parameters such as CRO and brine composition under reservoir conditions require attention. Overall, the surface chemistry of mineral phases in relation to factors such as temperature, pressure, and ambient fluids emerges as the key to understanding wettability phenomena in deep Earth conditions.

## References


Abdallah, W., Buckley, J. S., Carnegie, A. et al. 1986. Fundamentals of Wettability. *Technology* **38** (1125–1144): 268.

Abdallah, W. A. and Yang, Y. 2012. Raman Spectrum of Asphaltene. *Energy Fuels* **26** (11): 6888–6896. https://doi.org/10.1021/ef301247n.

Acevedo, S., Ranaudo, M. A., García, C. et al. 2000. Importance of Asphaltene Aggregation in Solution in Determining the Adsorption of This Sample on Mineral Surfaces. *Colloids Surf A* **166** (1–3): 145–152. https://doi.org/10.1016/S0927-7757(99)00502-6.

Alabi, O. O., Edilbi, A. N. F., Brolly, C. et al. 2015. Asphaltene Detection Using Surface Enhanced Raman Scattering (SERS). *Chem Commun* **51** (33): 7152–7155. https://doi.org/10.1039/C5CC00676G.

Al-Busaidi, I. K., Al-Maamari, R. S., Karimi, M. et al. 2019. Effect of Different Polar Organic Compounds on Wettability of Calcite Surfaces. *J Pet Sci Eng* **180**: 569–583. https://doi.org/10.1016/j.petrol.2019.05.080.

Alhammadi, A. M., AlRatrout, A., Singh, K. et al. 2017. In Situ Characterization of Mixed-Wettability in a Reservoir Rock at Subsurface Conditions. *Sci Rep* **7** (1): 10753. https://doi.org/10.1038/s41598-017-10992-w.

Anderson, W. G. 1986. Wettability Literature Survey—Part 1: Rock/Oil/Brine Interactions and the Effects of Core Handling and Wettability. *J Pet Technol* **38** (10): 1125–1144. SPE-13932-PA. https://doi.org/10.2118/13932-PA.

Andersson, M. P., Dideriksen, K., Sakuma, H. et al. 2016. Modelling How Incorporation of Divalent Cations Affects Calcite Wettability–Implications for Biomineralisation and Oil Recovery. *Sci Rep* **6**: 28854. https://doi.org/10.1038/srep28854.

Arvidson, R. S., Ertan, I. E., Amonette, J. E. et al. 2003. Variation in Calcite Dissolution Rates: A Fundamental Problem? *Geochim Cosmochim Acta* **67** (9): 1623–1634. https://doi.org/10.1016/S0016-7037(02)01177-8.

Arvidson, R. S. and Mackenzie, F. T. 1999. The Dolomite Problem; Control of Precipitation Kinetics by Temperature and Saturation State. *Am J Sci* **299** (4): 257–288. https://doi.org/10.2475/ajs.299.4.257.

Astilleros, J. M., Fernández-Díaz, L., and Putnis, A. 2010. The Role of Magnesium in the Growth of Calcite: An AFM Study. *Chem Geol* **271** (1–2): 52–58. https://doi.org/10.1016/j.chemgeo.2009.12.011.

Austad, T., Shariatpanahi, S. F., Strand, S. et al. 2012. Conditions for a Low-Salinity Enhanced Oil Recovery (EOR) Effect in Carbonate Oil Reservoirs. *Energy Fuels* **26** (1): 569–575. https://doi.org/10.1021/ef201435g.

Beens, J., Blomberg, J., and Schoenmakers, P. J. 2000. Proper Tuning of Comprehensive Two-Dimensional Gas Chromatography (GC× GC) to Optimize the Separation of Complex Oil Fractions. *J High Resolut Chromatogr* **23** (3): 182–188. https://doi.org/10.1002/(SICI)1521-4168(20000301)23:3<182::AID-JHRC182>3.0.CO;2-E.

Borromeo, L., Zimmermann, U., Andò, S. et al. 2017. Raman Spectroscopy as a Tool for Magnesium Estimation in Mg-Calcite. *J Raman Spectrosc* **48** (7): 983–992. https://doi.org/10.1002/jrs.5156.

Buckley, J. S. 2001. Effective Wettability of Minerals Exposed to Crude Oil. *Curr Opin Colloid Interface Sci* **6** (3): 191–196. https://doi.org/10.1016/S1359-0294(01)00083-8.

Cabane, B., Tournilhac, F., Geffroy, C. et al. 1997. The Frontier between Adsorption and Precipitation of Polyacrylic Acid on Calcium Carbonate. *Oil Gas Sci Technol* **52** (2): 183–190. https://doi.org/10.2516/ogst:1997017.

Cantrell, D., Swart, P., and Hagerty, R. 2004. Genesis and Characterization of Dolomite, Arab-D Reservoir, Ghawar Field, Saudi Arabia. *GeoArabia* **9** (2): 11–36.

Cantrell, D. L. and Hagerty, R. M. 1999. Microporosity in Arab Formation Carbonates, Saudi Arabia. *GeoArabia* **4** (2): 129–154.

Chen, S.-Y., Kaufman, Y., Kristiansen, K. et al. 2017. Effects of Salinity on Oil Recovery (the "Dilution Effect"): Experimental and Theoretical Studies of Crude Oil/Brine/Carbonate Surface Restructuring and Associated Physicochemical Interactions. *Energy Fuels* **31** (9): 8925–8941. https://doi.org/10.1021/acs.energyfuels.7b00869.

Coates, J. 2006. Interpretation of Infrared Spectra, A Practical Approach. In *Encyclopedia of Analytical Chemistry: Applications, Theory and Instrumentation*. New York, New York, USA: John Wiley & Sons.

Coelho, R. R., Hovell, I., Moreno, E. L. et al. 2007. Characterization of Functional Groups of Asphaltenes in Vacuum Residues Using Molecular Modelling and FTIR Techniques. *Pet Sci Technol* **25** (1–2): 41–54. https://doi.org/10.1080/10916460601054198.

Comans, R. N. J. and Middelburg, J. J. 1987. Sorption of Trace Metals on Calcite: Applicability of the Surface Precipitation Model. *Geochim Cosmochim Acta* **51** (9): 2587–2591. https://doi.org/10.1016/0016-7037(87)90309-7.

Cuiec, L. 1984. Rock/Crude-Oil Interactions and Wettability: An Attempt to Understand Their Interrelation. Paper presented at the SPE Annual Technical Conference and Exhibition, Houston, Texas, USA, 16–19 September. SPE-13211-MS. https://doi.org/10.2118/13211-MS.

Dai, Z., Kan, A. T., Shi, W. et al. 2017. Solubility Measurements and Predictions of Gypsum, Anhydrite, and Calcite Over Wide Ranges of Temperature, Pressure, and Ionic Strength with Mixed Electrolytes. *Rock Mech Rock Eng* **50:** 327–339. https://doi.org/10.1007/s00603-016-1123-9.

Eftekhardadkhah, M., Kløcker, K. N., Trapnes, H. H. et al. 2016. Composition and Dynamic Adsorption of Crude Oil Components Dissolved in Synthetic Produced Water at Different pH Values. *Ind Eng Chem Res* **55** (11): 3084–3090. https://doi.org/10.1021/acs.iecr.5b04459.

Eisenlohr, L., Meteva, K., Gabrovšek, F. et al. 1999. The Inhibiting Action of Intrinsic Impurities in Natural Calcium Carbonate Minerals to Their Dissolution Kinetics in Aqueous $H_2O$–$CO_2$ Solutions. *Geochim Cosmochim Acta* **63** (7–8): 989–1001. https://doi.org/10.1016/S0016-7037(98)00301-9.

Elhadj, S., Salter, E. A., Wierzbicki, A. et al. 2006. Peptide Controls on Calcite Mineralization: Polyaspartate Chain Length Affects Growth Kinetics and Acts as a Stereochemical Switch on Morphology. *Cryst Growth Des* **6** (1): 197–201. https://doi.org/10.1021/cg050288+.

England, W. A. 2007. Reservoir Geochemistry—A Reservoir Engineering Perspective. *J Pet Sci Eng* **58** (3–4): 344–354. https://doi.org/10.1016/j.petrol.2005.12.012.

Fathi, S. J., Austad, T., and Strand, S. 2011. Water-Based Enhanced Oil Recovery (EOR) by "Smart Water": Optimal Ionic Composition for EOR in Carbonates. *Energy Fuels* **25** (11): 5173–5179. https://doi.org/10.1021/ef201019k.

Frye, G. C. and Thomas, M. M. 1993. Adsorption of Organic Compounds on Carbonate Minerals: 2. Extraction of Carboxylic Acids from Recent and Ancient Carbonates. *Chem Geol* **109** (1–4): 215–226. https://doi.org/10.1016/0009-2541(93)90071-P.

González, G. and Moreira, M. B. C. 1991. The Wettability of Mineral Surfaces Containing Adsorbed Asphaltene. *Colloids Surf* **58** (3): 293–302. https://doi.org/10.1016/0166-6622(91)80229-H.

Gunasekaran, S., Anbalagan, G., and Pandi, S. 2006. Raman and Infrared Spectra of Carbonates of Calcite Structure. *J Raman Spectrosc* **37** (9): 892–899. https://doi.org/10.1002/jrs.1518.

Hefter, G. T. and Tomkins, R. P. 2003. *The Experimental Determination of Solubilities*. New York, New York, USA: John Wiley & Sons.

Helgeson, H. C., Knox, A. M., Owens, C. E. et al. 1993. Petroleum, Oil Field Waters, and Authigenic Mineral Assemblages are They in Metastable Equilibrium in Hydrocarbon Reservoirs. *Geochim Cosmochim Acta* **57** (14): 3295–3339. https://doi.org/10.1016/0016-7037(93)90541-4.

Hirasaki, G. and Zhang, D. L. 2004. Surface Chemistry of Oil Recovery from Fractured, Oil-Wet, Carbonate Formations. *SPE J*. **9** (2): 151–162. SPE-88365-PA. https://doi.org/10.2118/88365-PA.

Hirschberg, A. 1988. Role of Asphaltenes in Compositional Grading of a Reservoir's Fluid Column. *J Pet Technol* **40** (1): 89–94. SPE-13171-PA. https://doi.org/10.2118/13171-PA.

Hirschberg, A., deJong, L. N. J., Schipper, B. A. et al. 1984. Influence of Temperature and Pressure on Asphaltene Flocculation. *SPE J*. **24** (3): 283–293. SPE-11202-PA. https://doi.org/10.2118/11202-PA.

Hjelmeland, O. S. and Larrondo, L. E. 1986. Experimental Investigation of the Effects of Temperature, Pressure, and Crude Oil Composition on Interfacial Properties. *SPE Res Eng* **1** (4): 321–328. SPE-12124-PA. https://doi.org/10.2118/12124-PA.

Hong, L., Teng, M., Xiucheng, T. et al. 2016. Origin of Structurally Controlled Hydrothermal Dolomite in Epigenetic Karst System during Shallow Burial: An Example from Middle Permian Maokou Formation, Central Sichuan Basin, SW China. *Pet Explor Dev* **43** (6): 1000–1012. https://doi.org/10.1016/S1876-3804(16)30117-3.

Huang, Y.-C., Gindele, M. B., Knaus, J. et al. 2018. On Mechanisms of Mesocrystal Formation: Magnesium Ions and Water Environments Regulate the Crystallization of Amorphous Minerals. *CrystEngComm* **20** (31): 4395–4405. https://doi.org/10.1039/C8CE00241J.

Hutin, A., Argillier, J.-F., and Langevin, D. 2014. Mass Transfer between Crude Oil and Water. Part 1: Effect of Oil Components. *Energy Fuels* **28** (12): 7331–7336. https://doi.org/10.1021/ef501751b.

Ivanova, A., Mitiurev, N., Cheremisin, A. et al. 2019a. Characterization of Organic Layer in Oil Carbonate Reservoir Rocks and Its Effect on Microscale Wetting Properties. *Sci Rep* **9**: 10667. https://doi.org/10.1038/s41598-019-47139-y.

Ivanova, A., Orlov, D., Mitiurev, N. et al. 2019b. Microstructural Imaging and Characterization of Organic Matter Presented in Carbonate Oil Reservoirs. Paper presented at the SPE Europec Featured at 81st EAGE Conference and Exhibition, London, England, UK, 3–6 June. SPE-195456-MS. https://doi.org/10.2118/195456-MS.

Jackson, M. D., Al-Mahrouqi, D., and Vinogradov, J. 2016. Zeta Potential in Oil-Water-Carbonate Systems and Its Impact on Oil Recovery during Controlled Salinity Water-Flooding. *Sci Rep* **6**: 37363. https://doi.org/10.1038/srep37363.

Jadhunandan, P. P. and Morrow, N. R. 1995. Effect of Wettability on Waterflood Recovery for Crude-Oil/Brine/Rock Systems. *SPE Res Eng* **10** (1): 40–46. SPE-22597-PA. https://doi.org/10.2118/22597-PA.

Jawhari, T., Roid, A., and Casado, J. 1995. Raman Spectroscopic Characterization of Some Commercially Available Carbon Black Materials. *Carbon* **33** (11): 1561–1565. https://doi.org/10.1016/0008-6223(95)00117-V.

Jehlička, J., Urban, O., and Pokorný, J. 2003. Raman Spectroscopy of Carbon and Solid Bitumens in Sedimentary and Metamorphic Rocks. *Spectrochim Acta, Part A* **59** (10): 2341–2352. https://doi.org/10.1016/S1386-1425(03)00077-5.

Jonas, L., Müller, T., Dohmen, R. et al. 2015. Transport-Controlled Hydrothermal Replacement of Calcite by Mg-Carbonates. *Geology* **43** (9): 779–782. https://doi.org/10.1130/G36934.1.

Joonaki, E., Buckman, J., Burgass, R. et al. 2019. Water Versus Asphaltenes; Liquid–Liquid and Solid–Liquid Molecular Interactions Unravel the Mechanisms behind an Improved Oil Recovery Methodology. *Sci Rep* **9**: 11369. https://doi.org/10.1038/s41598-019-47782-5.

Kelemen, S. R. and Fang, H. L. 2001. Maturity Trends in Raman Spectra from Kerogen and Coal. *Energy Fuels* **15** (3): 653–658. https://doi.org/10.1021/ef0002039.

Khatabi, S., Ostadhassan, M., and Aghajanpour, A. 2018. Raman Spectroscopy: An Analytical Tool for Evaluating Organic Matter. *J Oil Gas Petrochem Sci* **1** (1): 28–33. https://doi.org/10.30881/jogps.00007.

Klemme, H. D. and Ulmishek, G. F. 1991. Effective Petroleum Source Rocks of the World: Stratigraphic Distribution and Controlling Depositional Factors. *AAPG Bull* **75** (12): 1809–1851. https://doi.org/10.1306/0C9B2A47-1710-11D7-8645000102C1865D.

Kumar, K., Dao, E., and Mohanty, K. K. 2005. AFM Study of Mineral Wettability with Reservoir Oils. *J Colloid Interface Sci* **289** (1): 206–217. https://doi.org/10.1016/j.jcis.2005.03.030.

Lahann, R. W. and Campbell, R. C. 1980. Adsorption of Palmitic Acid on Calcite. *Geochim Cosmochim Acta* **44** (5): 629–634. https://doi.org/10.1016/0016-7037(80)90152-0.

Larter, S. R., Aplin, A. C., Corbett, P. W. M. et al. 1997. Reservoir Geochemistry: A Link between Reservoir Geology and Engineering? *SPE Res Eng* **12** (1): 12–17. SPE-28849-PA. https://doi.org/10.2118/28849-PA.

Lashkarbolooki, M., Riazi, M., Hajibagheri, F. et al. 2016. Low Salinity Injection into Asphaltenic-Carbonate Oil Reservoir, Mechanistical Study. *J Mol Liq* **216**: 377–386. https://doi.org/10.1016/j.molliq.2016.01.051.

Lopez, O., Zuddas, P., and Faivre, D. 2009. The Influence of Temperature and Seawater Composition on Calcite Crystal Growth Mechanisms and Kinetics: Implications for Mg Incorporation in Calcite Lattice. *Geochim Cosmochim Acta* **73** (2): 337–347. https://doi.org/10.1016/j.gca.2008.10.022.

Lu, Y., Najafabadi, N. F., and Firoozabadi, A. 2017. Effect of Temperature on Wettability of Oil/Brine/Rock Systems. *Energy Fuels* **31** (5): 4989–4995. https://doi.org/10.1021/acs.energyfuels.7b00370.

Maqbool, T., Srikiratiwong, P., and Fogler, H. S. 2011. Effect of Temperature on the Precipitation Kinetics of Asphaltenes. *Energy Fuels* **25** (2): 694–700. https://doi.org/10.1021/ef101112r.

Marshall, A. G. and Rodgers, R. P. 2008. Petroleomics: Chemistry of the Underworld. *PNAS* **105** (47): 18090–18095. https://doi.org/10.1073/pnas.0805069105.

Mason, R. A. and Mariano, A. N. 1990. Cathodoluminescence Activation in Manganese-Bearing and Rare Earth-Bearing Synthetic Calcites. *Chem Geol* **88** (1–2): 191–206. https://doi.org/10.1016/0009-2541(90)90113-L.

Montel, F., Bickert, J., Hy-Billiot, J. et al. 2003. Pressure and Compositional Gradients in Reservoirs. Paper presented at the Nigeria Annual International Conference and Exhibition, Abuja, Nigeria, 4–6 August. SPE-85668-MS. https://doi.org/10.2118/85668-MS.

Moore, C. H. 1989. *Carbonate Diagenesis and Porosity*, Vol. 46. Amsterdam, The Netherlands: Elsevier.

Moore, C. H. and Wade, W. J. 2013. *Carbonate Reservoirs: Porosity and Diagenesis in a Sequence Stratigraphic Framework*, Vol. 67. Waltham, Massachusetts, USA: Academic Press.

Morrow, N. R. 1990. Wettability and Its Effect on Oil Recovery. *J Pet Technol* **42** (12): 1476–1484. SPE-21621-PA. https://doi.org/10.2118/21621-PA.

Nair, S., Gao, J., Yao, Q. et al. 2020. Algorithm-Improved High Speed and Non-Invasive Confocal Raman Imaging of Two-Dimensional Materials. *Natl Sci Rev* **7** (3): 620–628. https://doi.org/10.1093/nsr/nwz177.

Niebergall, P. J. and Sugita, E. T. 1968. Utilization of the Guggenheim Method in Kinetics. *J Pharma Sci* **57** (10): 1805–1808. https://doi.org/10.1002/jps.2600571045.

Noiriel, C., Oursin, M., Saldi, G. et al. 2019. Direct Determination of Dissolution Rates at Crystal Surfaces Using 3D X-Ray Microtomography. *ACS Earth Space Chem* **3** (1): 100–108. https://doi.org/10.1021/acsearthspacechem.8b00143.

Orme, C. A., Noy, A., Wierzbicki, A. et al. 2001. Formation of Chiral Morphologies through Selective Binding of Amino Acids to Calcite Surface Steps. *Nature* **411** (6839): 775–779. https://doi.org/10.1038/35081034.

Peters, K. E. and Fowler, M. G. 2002. Applications of Petroleum Geochemistry to Exploration and Reservoir Management. *Org Geochem* **33** (1): 5–36. https://doi.org/10.1016/S0146-6380(01)00125-5.

Piro, G., Canonico, L. B., Galbariggi, G. et al. 1996. Asphaltene Adsorption onto Formation Rock: An Approach to Asphaltene Formation Damage Prevention. *SPE Prod & Fac* **11** (3): 156–160. SPE-30109-PA. https://doi.org/10.2118/30109-PA.

Plummer, L. N. and Busenburg, E. 1982. The Solubilities of Calcite, Aragonite and Vaterite in $CO_2$-$H_2O$ Solutions between 0 and 90°C, and an Evaluation of the Aqueous Model for the System $CaCO_3$-$CO_2$-$H_2O$. *Geochimica et Cosmochimica Acta* **46** (6): 1011–1040. https://doi.org/10.1016/0016-7037(82)90056-4.

Putnis, A. 2009. Mineral Replacement Reactions. *Rev Miner Geochem* **70** (1): 87–124. https://doi.org/10.2138/rmg.2009.70.3.

Rao, A., Kumar, S., Annink, C. et al. 2020. Mineral Interfaces and Oil Recovery: A Microscopic View on Surface Reconstruction, Organic Modification, and Wettability Alteration of Carbonates. *Energy Fuels* **34** (5): 5611–5622. https://doi.org/10.1021/acs.energyfuels.0c00118.

Rodriguez-Navarro, C., Burgos Cara, A., Elert, K. et al. 2016. Direct Nanoscale Imaging Reveals the Growth of Calcite Crystals via Amorphous Nanoparticles. *Cryst Growth Des* **16** (4): 1850–1860. https://doi.org/10.1021/acs.cgd.5b01180.

Sakuma, H., Andersson, M. P., Bechgaard, K. et al. 2014. Surface Tension Alteration on Calcite, Induced by Ion Substitution. *J Phys Chem C* **118** (6): 3078–3087. https://doi.org/10.1021/jp411151u.

Saraji, S., Goual, L., and Piri, M. 2013. Dynamic Adsorption of Asphaltenes on Quartz and Calcite Packs in the Presence of Brine Films. *Colloids Surf A* **434**: 260–267. https://doi.org/10.1016/j.colsurfa.2013.05.070.

Sari, A., Al Maskari, N. S., Saeedi, A. et al. 2020. Impact of Surface Roughness on Wettability of Oil-Brine-Calcite System at Sub-Pore Scale. *J Mol Liq* **299**: 112107. https://doi.org/10.1016/j.molliq.2019.112107.

Sayyouh, M. H., Hemeida, A. M., Al-Blehed, M. S. et al. 1991. Role of Polar Compounds in Crude Oils on Rock Wettability. *J Pet Sci Eng* **6** (3): 225–233. https://doi.org/10.1016/0920-4105(91)90015-F.

Schmoker, J. W., Krystinik, K. B., and Halley, R. B. 1985. Selected Characteristics of Limestone and Dolomite Reservoirs in the United States. *AAPG Bull* **69** (5): 733–741. https://doi.org/10.1306/AD4627F9-16F7-11D7-8645000102C1865D.

Shah, D. O. 2012. *Improved Oil Recovery by Surfactant and Polymer Flooding*. Amsterdam, The Netherlands: Elsevier.

Shiu, W. Y., Bobra, M., Bobra, A. M. et al. 1990. The Water Solubility of Crude Oils and Petroleum Products. *Oil Chem Pollut* **7** (1): 57–84. https://doi.org/10.1016/S0269-8579(05)80034-6.

Sørgård, H. N., Totland, C., Nerdal, W. et al. 2017. Crude Oil Adsorbates on Calcite and Quartz Surfaces Investigated by NMR Spectroscopy. *J Phys Chem C* **121** (38): 20892–20899. https://doi.org/10.1021/acs.jpcc.7b07125.

Stipp, S. L. and Hochella, M. F. Jr. 1991. Structure and Bonding Environments at the Calcite Surface as Observed with X-Ray Photoelectron Spectroscopy (XPS) and Low Energy Electron Diffraction (LEED). *Geochim Cosmochim Acta* **55** (6): 1723–1736. https://doi.org/10.1016/0016-7037(91)90142-R.

Strausz, O. P., Safarik, I., and Lown, E. M. 2009. Cause of Asphaltene Fluorescence Intensity Variation with Molecular Weight and Its Ramifications for Laser Ionization Mass Spectrometry. *Energy Fuels* **23** (3): 1555–1562. https://doi.org/10.1021/ef800480y.

Subramanian, S., Sørland, G. H., Simon, S. et al. 2017. Asphaltene Fractionation Based on Adsorption onto Calcium Carbonate: Part 2. Self-Association and Aggregation Properties. *Colloids Surf A* **514**: 79–90. https://doi.org/10.1016/j.colsurfa.2016.11.035.

Sun, S. Q. 1995. Dolomite Reservoirs: Porosity Evolution and Reservoir Characteristics. *AAPG Bull* **79** (2): 186–204. https://doi.org/10.1306/8D2B14EE-171E-11D7-8645000102C1865D.

Sun, W., Jayaraman, S., Chen, W. et al. 2015. Nucleation of Metastable Aragonite $CaCO_3$ in Seawater. *PNAS* **112** (11): 3199–3204. https://doi.org/10.1073/pnas.1423898112.

Thomas, M. M., Clouse, J. A., and Longo, J. M. 1993a. Adsorption of Organic Compounds on Carbonate Minerals: 1. Model Compounds and Their Influence on Mineral Wettability. *Chem Geol* **109** (1–4): 201–213. https://doi.org/10.1016/0009-2541(93)90070-Y.

Thomas, M. M., Clouse, J. A., and Longo, J. M. 1993b. Adsorption of Organic Compounds on Carbonate Minerals: 3. Influence on Dissolution Rates. *Chem Geol* **109** (1–4): 227–237. https://doi.org/10.1016/0009-2541(93)90072-Q.

Vavouraki, A. I., Putnis, C. V., Putnis, A. et al. 2008. An Atomic Force Microscopy Study of the Growth of Calcite in the Presence of Sodium Sulfate. *Chem Geol* **253** (3–4): 243–251. https://doi.org/10.1016/j.chemgeo.2008.05.013.

Wood, S., Hollis, J. R., and Kim, J.-S. 2017. Raman Spectroscopy as an Advanced Structural Nanoprobe for Conjugated Molecular Semiconductors. *J Phys D: App Phys* **50** (7): 073001. https://doi.org/10.1088/1361-6463/50/7/073001.

Xu, J., Wang, J., Hong, M. et al. 2016. Solution-Chemistry Control of $Mg^{2+}$-Calcite Interaction Mechanisms: Implication for Biomineralization. *Am Miner* **101** (5): 1104–1112. https://doi.org/10.2138/am-2016-5406.

Young, C. A. and Miller, J. D. 2000. Effect of Temperature on Oleate Adsorption at a Calcite Surface: An FT-NIR/IRS Study and Review. *Int J Miner Process* **58** (1–4): 331–350. https://doi.org/10.1016/S0301-7516(99)00057-5.

Yousef, A. A., Al-Saleh, S. H., Al-Kaabi, A. et al. 2011. Laboratory Investigation of the Impact of Injection-Water Salinity and Ionic Content on Oil Recovery from Carbonate Reservoirs. *SPE Res Eval & Eng* **14** (5): 578–593. SPE-137634-PA. https://doi.org/10.2118/137634-PA.

Yu, L. and Buckley, J. S. 1997. Evolution of Wetting Alteration by Adsorption from Crude Oil. *SPE Form Eval* **12** (1): 5–12. SPE-28970-PA. https://doi.org/10.2118/28970-PA.

Yutkin, M. P., Mishra, H., Patzek, T. W. et al. 2018. Bulk and Surface Aqueous Speciation of Calcite: Implications for Low-Salinity Waterflooding of Carbonate Reservoirs. *SPE J*. **23** (1): 84–101. SPE-182829-PA. https://doi.org/10.2118/182829-PA.